PULSE SHAPE DISCRIMINATION OF LIQUID SCINTILLATORS

Gioacchino Ranucci[1]*, Augusto Goretti, Paolo Lombardi*
Istituto Nazionale di Fisica Nucleare, via Celoria 16, I-20133 Milano

In this paper we describe the results of different techniques applied to characterize experimentally the pulse shape discrimination capability of liquid scintillators. A detailed comparison of the results obtained with each method is reported, together with the description of an optimization strategy which can be adopted to obtain the best exploitation of the intrinsic PSD feature of the scintillator samples.
Keywords: pulse shape discrimination; liquid scintillator detectors; single photon sampling technique.
PACS : 29.40.M

[1] Corresponding author
tel: +39 2 2392362
fax +39 2 2392617
email: ranucci@mi.infn.it

1. Introduction

Pulse shape discrimination is a key property in many applications involving liquid scintillators. It is very often used to discriminate the desired signal against the unwanted background which is affecting the measurement. Applications for neutron/gamma separation have been thoroughly described in the literature over the past 30 years [1], [2]. More recently a widespread interest emerged for PSD exploitation in phoswitch detectors for X-rays detection [3]. Another area of interest which has gained special attention is that of massive detectors for detection of rare events [4]. Here the PSD is exploited to identify the alpha induced signals produced by the natural radioactivity (essentially ^{238}U and ^{232}Th). Such an application is foreseen to be intensively adopted in the low energy solar neutrino experiment Borexino [5], where it will allow to disentangle the true neutrino signal, due to the scattering interaction on the electrons of the scintillator, from the alpha background events.

This work describes the results obtained through the exploitation of two different methods for the evaluation of the α/β discrimination capability of liquid scintillators on small scale laboratory samples. The measurements have been performed on candidate mixtures for the low energy solar neutrino detector Borexino, as well as on the standard NE213 scintillator, specifically optimized for the PSD application. The description of the results will be complemented by a comparison of the characterization obtained with the two different methods. A procedure to optimize the PSD performances will be also illustrated.

2. Procedures of evaluation of the alpha/beta properties

In order to evaluate the alpha/beta properties two approaches have been exploited, one indirect and the other direct.

In the former the pulse shape of the scintillation light induced by α and β particles has been derived experimentally through the application of the so called "single-photon sampling technique" [6], [7]. Therefore, on the basis of the measured waveshapes it is possible to compute the alpha/beta discrimination performances which can be obtained. Obviously, the achievable discrimination depends upon the type of processing applied to exploit the basic pulse shape difference existing between α and β pulses. In the practical implementations the PSD is carried out through either the so called rise time approach or the charge integration technique [8], [9], [10]. Both procedures are

suboptimal methods with respect to the optimal one due to Gatti and Svelto, which is described in [11]. Here we have followed the charge approach, which assures better performances with respect to the rise time method, as shown in [10] and [12], and leads also to a simpler and straightforward implementation.

We remind that the processing procedure implied by the charge method consists in measuring both the total charge associated with the pulse at the output of the photomultiplier and the charge in its tail. These two quantities are used to compute the tail-to-total charge ratio, which is the separation parameter assumed as discrimination factor between α's and β's, in the sense that if the charge ratio is less than a properly adjusted discrimination threshold the pulse is attributed to a β, otherwise it is interpreted as that of an α.

In paragraph 3 we refer to the description of the experimental features of the "single-photon sampling technique" already given [13], as well as to the experimental set-up illustrated there. In addition, we give a thorough a discussion about the effect of the dissolved oxygen in the scintillator sample, which is crucial for a proper evaluation of the scintillation tail and thus of the PSD.

In paragraph 4 and 5 two procedures are illustrated to determine the PSD properties from the measured light waveshape. Specifically, in paragraph 4 an approximated analytical approach is described, while in paragraph 5 a more complete Monte Carlo method is illustrated. In both cases the predictions lead to a quantitative assessment of the degree of discrimination achievable through the exploitation of the charge method.

On the other hand, the direct characterization method consists simply in the application to the pulses originated in a scintillator sample by a known α or β source of the charge approach processing.

The experimental set-up which has been implemented to carry out the direct measurement is described in paragraph 6, together with the results obtained with it.

Finally, in paragraph 7 we report the comparison between the prediction of the degree of α/β discrimination inferred by the measured pulse shape and the results originated by the direct measurements.

3. Pulse waveshape determination for the application of the indirect approach

The experimental set-up for this kind of measurements, already described in [13], has been slightly modified to perform the present investigation in order to improve the

quality of the data. The most important change concerned the low level photomultiplier: the one which is used now is characterized by a very low dark count rate, of the order of 0.5 Hz, hence originating a negligible random coincidence rate. As a consequence it was possible to extend the span of the measurement up to 1.6 μs, in order to detect also a weak, long tail, while previously the measurements spanned over an interval limited to 500 ns.

Additionally, the new device, being of the side-window type, is not affected from the bump effect which appeared in the previous measurements located 20 ns after the main peak.

Finally, we removed from the measurements some electronic artifacts, which produced small wiggles superimposed on the smooth shape of the measured curves.

It is important to underline that such measurements are strongly affected by the presence of oxygen dissolved in the liquid. Indeed, it is well known that oxygen produces contact compounds with the scintillator molecules, originating the twofold effect of reducing both the overall light yield and the relative amount of light in the slow component of the light pulse [14]. It is thus essential to remove completely oxygen traces in the mixture under test by thoroughly sparging the sample with nitrogen.

The effectiveness of such a procedure has been tested by flushing the vial containing the scintillating cocktail for different time, obtaining the curves displayed in figure 1. The lowest curve is the scintillation decay with no nitrogen flushing at all, while the others are obtained with increasing flushing periods of 10, 30 and 60 minutes. The net effect of the increasing flushing time is a clearer appearance of the tail, which reaches its final value after 30 minutes of nitrogen purging. Indeed, the two curves obtained with 30 and 60 minutes of flushing are completely overlapped (it is even impossible to distinguish them in the figure), indicating the accomplishment of total oxygen removal.

In figure 2, 3 and 4 we report the results of the measurements obtained respectively on two possible candidates for the Borexino scintillator, i.e. two mixtures of Pseudocumene and PPO, with the PPO dissolved at the level of 1.5 g/l and 6g/l, and on the standard NE213 scintillator. In all the figures the responses of the scintillating cocktails to α and β excitations are displayed together.

We remind that the measurements are affected by the finite resolution function of the set-up, essentially due to the transit time spread featured by the tubes used to detect

the scintillation photons. It is thus important to adopt a proper procedure to calibrate the resolution function and to use it to correct the raw data, as already explained in [13].

Quantitatively the curves can be described as a sum of exponential term, i.e.

$$\sum_{i=1}^{n} \frac{q_i}{\tau_i} e^{-\frac{t}{\tau_i}}$$

where the q_i represent the weight of each term.

In the table I and II the various q_i and τ_i factors, obtained after taking into account the resolution effect, are shown for β and α irradiation respectively. They give the quantitative description of the average pulse shapes upon which the analysis to determine the PSD properties of the scintillators is based.

Before going on, however, it should be clarified that only the first component has an intrinsic meaning, being determined by the concurrent effect of the lifetime of the scintillating molecular state and of the energy transfer between the solvent and the solute. The other components account only for a simple mathematical description of the tail.

4. Exploitation of the light pulse shape for the prediction of the PSD performances

With the light waveshape measured as explained in the previous paragraph, the prediction of the PSD performances of the scintillator can be carried out, given a specific pulse height, i.e. the number of photoelectrons forming the pulse, by determining quantitatively the distribution of the charge signal in the tail for the alpha and beta pulses, and then by determining their degree of overlap. The overlap is quantified by evaluating the factor of merit parameter D, which is normally adopted for this purpose [10], defined as

$$D = \Delta S / (\sigma_e^2 + \sigma_\alpha^2)^{1/2}$$

In a first approximation, we can compute the charge distribution in the tail as the distribution of the number of photoelectrons emitted after a properly defined elapsing time from the beginning of the pulse. In such a way the problem is reduced to the determination of two binomial distributions, one for the α's and the other for the β's.

The probability density function of the time of production of a photoelectron is equal to the convolution of the scintillation light shape with the transit time jitter of the photomultiplier [15]. On such a curve we can consider conventionally a time at which the tail starts.

Hence, by computing the ratio of the area under the conventional tail to the total area of the curve we obtain the probability of a photoelectron to be emitted in the tail itself. The beginning time of the tail is to be considered as a parameter, whose choice can be based upon the maximization of the achievable discrimination.

If p is the probability of emission in the tail, and n is the total number of photoelectrons in the pulse, then the probability of having k photoelectrons in the tail is given by the binomial expression:

$$p_{tail}(k) = \binom{n}{k} p^k (1-p)^{n-k}$$

As an example, the two distributions obtained for α and β particles for the PC+PPO scintillator (1.5 g/l), assuming a conventional start of the tail at 25 ns, for a total pulse height of 100 photoelectrons and for a global integration time of 500 ns are displayed in figure 5. In the abscissa instead of the number of photoelectrons in the tail we report the ratio between the total number of photoelectrons and those in the tail itself.

The optimization of the choice of both the integration time and the beginning of the tail can be carried out by studying the dependence upon them of the factor of merit D. In figure 6, 7, 8 the values of D of the three measured scintillators, for various integration time, for different beginning of the tails, and for a fixed pulse height of 100 photoelectrons are reported, from which it emerges that the best value for the start of the tail is equal to 20 ns for the first, to 14 ns for the second and to 18 ns for the last.

From the same figures it can be inferred that the longer the integration time, the better the result which can be obtained. This circumstance is better shown in the figure 9, where the D parameter is reported as function of integration time for the PC+PPO (1.5 g/l) mixture, in the case of the tail of 20 ns and for 100 photoelectrons. From this plot it can be concluded that the D parameter initially is strongly dependent upon the length of the integration gate, reaching however very soon a saturation condition in which additional increases of the integration time produce only marginal improvements to the discrimination capability. In particular we can assume that an integration time of 500 ns is adequate to obtain a good PSD.

It must be pointed out that while the maximum value of the factor of merit D is depending upon the pulse height, i.e. the number of photoelectrons in the pulse, the optimum beginning of the tail and the effect of the length of the integration gate are independent from the pulse height itself. This circumstance has been checked by performing the calculation for different number of photoelectrons in the pulse, as shown in figure 10 for the case of 200 photoelectrons for the PC+PPO (1.5 g/l) scintillator.

Finally, in figure 11 we report the maximum value of the D factor for the optimum tail of 20 ns and for the integration gate of 500 ns, plotted as function of the number of photoelectrons, in the case of the PC+PPO (1.5 g/l) scintillator. As expected, D varies proportionally to the square root of the number of photoelectrons, as shown by the perfect overlap of the circles indicating the calculated points and the solid line representing a function proportional to $\sqrt{N_{pe}}$.

5. Effect of the photomultiplier characteristics

In the previous paragraph we have described a way to evaluate quantitatively the intrinsic PSD properties of a scintillator, taking into account among the effects related to the phototube only the transit time jitter.

Actually the shape of the anode pulse is determined also by the overall response of the phototube to the photons. In order to evaluate in which way the intrinsic features of the device modifies the PSD, a Monte Carlo modeling has been carried out, following the procedures outlined in [16] and [17]. In this calculation the purpose was to determine, for each event, the ratio of the charge in the tail to that in the whole pulse in the simulated waveform. Hence by carrying out the simulation for a large number of α and β events, we obtained the distributions of the charge ratio for the two kinds of pulse among which the discrimination must be carried out. From these distributions it is possible to determine the D factor of merit.

In doing the Monte Carlo according to the prescription in [17], the single photoelectron anode pulse, its amplitude distribution and the transit time jitter have been taken from the experimental characterization performed on a RCA 8850 phototube used for the direct application of the charge method described in the following paragraphs 6 and 7.

In figures 12 these three curves experimentally detected are reported.

We briefly remind here that the Monte Carlo procedure implies to generate a time of emission of the photon according to the light profile of the scintillation pulse and to add a second time representing the transit time jitter of the device's response. The overall time obtained in such a way represents the time of production of a anode pulse. Then, starting from that point it is assumed the production of the relevant anode pulse whose shape is fixed and equal to the profile reported in figure 12 b, while its amplitude is distributed according to the curve in figure 12 a. After repeating this procedure for all the photoelectrons comprised in the pulse, the individual responses to each of them are summed together to obtain the overall anode pulse, which is afterward processed to derive the tail-to-total charge ratio.

Some typical waveforms obtained with this procedure are reported in figure 13, while in figure 14 the α and β charge ratio distributions obtained for pulses comprising in total 100 photoelectrons are reported, in the case of PC+PPO (1.5 g/l), computed for an integration gate of 500 ns and a tail starting time of 25 ns.

In figure 15 we report for the PC+PPO (1.5 g/l) scintillator, the mean value of both alpha and beta charge ratio distributions, as function of the conventional beginning of the tail, compared to the value obtained with the approximated analytical procedure described in the previous paragraph. It can be noted that the two values differ in a significant way for early starts of the tail, while they asymptotically coincides when the beginning of the tail is delayed.

In figure 16, 17 and 18 the D parameter obtained for the PC+PPO (1.5 g/l), the PC+PPO (6g/l) and the NE213 scintillators are shown, as function of the definition of the tail and for different integration gates, and for a pulse height of 100 photoelectrons. From these calculations we can infer that in each of these three cases the optimum beginning of the tail is shifted with respect to the value obtained with the procedure of the previous paragraph. On the other hand, it is confirmed that increasing the length of the gate the discrimination capability increases. In addition, we can note that the maximum of the D parameter is lower than in the previous calculation. Such differences are very evident in the comparison shown in figure 19 between the D parameter for PC+PPO (1.5 g/l) evaluated with the two procedures, for the same integration gate of 500 ns: in the former evaluation the optimum tail start at 20 ns, while in the latter it is equal to 26 ns, and the maximum of the D factor is reduced from the original value of 2.90 to the final one of 2.69.

Finally, in figure 20 the maximum value of the D parameter, evaluated as function of the number of photoelectrons, is reported for the PC+PPO (1.5 g/l) scintillator, compared to the value predicted with the previous analytical calculation. From this plot we can conclude that the overall effect of the phototube is to reduce the intrinsic PSD capability of the scintillator, even though not drastically.

6. Direct approach

The test set-up realized to measure directly, under alpha and beta irradiation, the amount of light emitted in the tail is shown in figure 21. A small quartz vial is located on the faceplate of a photomultiplier and coupled to it in such a way that the mean number of detected photoelectrons can be properly adjusted. Several replicas of the analog signal produced by the photomultiplier are obtained by a fan-out; they are routed, differently delayed each other, to the inputs of respectively a charge ADC and a constant fraction discriminator, which is used to derive the gate integration signal needed to collect the charge of the pulse. With this arrangement it is possible to measure the charge for different definitions of the starting point of the tail.

Furthermore, different measurements have been carried out changing the overall length of the integration window. In such a way it has been possible to perform experimentally the same kind of optimization procedure performed in paragraph 4 and 5 numerically.

The results of the measurements are plotted as scatterplot according to the format shown in figure 22 and 23, where the tail-to-total ratio is reported as function of the number of photoelectrons both for the PC+PPO (1.5 g/l) scintillator and the NE213, together with the projection on the y axis, limited to the interval from 160 to 180 photoelectrons, evaluated with an integration gate of 500 ns and a tail starting time at 20 ns after the beginning of the pulse. In particular from this projection it is possible to compute the D parameter, which is reported in the figures.

The result of the experimental optimizations performed on the PC+PPO (1.5 g/l) scintillator and the NE213 are reported in figures 24 and 25 respectively.

These data confirm on one hand a strong dependence of the D parameter on the definition of the starting point of the tail, and on the other the less pronounced dependence upon the total integration time, hence showing qualitatively the same

trends predicted in the paragraphs 4 and 5. A careful and quantitative comparison is carried out in the next paragraph.

7. Comparison of the results obtained with the two methods

A quantitative comparison between the experimental data and the simulations requires a precise evaluation of the number of photoelectrons.

In the measurements whose results have been described in the previous paragraph we used a photomultiplier not showing a pronounced single photoelectron peak. Hence, to be more sure about the evaluation of the number of photoelectrons, we modified our set-up by replacing the previous photomultiplier with a RCA 8850 phototube, featuring a very well defined single photoelectron peak and thus allowing a careful determination of how many photoelectrons are comprised in the pulse. In view of this comparison, the characteristics of this phototube have been used for the Monte Carlo evaluation of paragraph 5.

The final set of measurements to perform the comparison were carried out only for the PC+PPO (1.5 g/l) mixture.

A first comparison is shown in figure 26, where the measured and calculated α and β ratio charge distribution, with an integration gate of 500 ns, and a start of the tail of 25 ns, are overlapped. Both the Monte Carlo data and the experimental results are relevant to the range from 140 to 160 photoelectrons.

It must be pointed out that the Monte Carlo evaluation for this comparison has been carried out not for a fixed number of photoelectrons in the pulse, as in paragraph 5, but assuming for the beta spectrum a uniform pulse height distribution from 140 to 160 photoelectrons and for the α a Poisson distribution centered at 150 photoelectrons. With this choice the simulation is performed in accordance to the actual conditions of the direct measurement.

Figure 26 demonstrates that the agreement between the experimental data and the Monte Carlo prediction is good, with only a slight shift between the calculated and simulated distributions.

A further comparison is shown in figure 27, where the solid line is the Monte Carlo evaluated D parameter as function of the tail starting time, and the circles represent four experimental data. In the figure we report the error on both the determinations of D, which is of the order of ± 0.07.

The agreement is excellent for the first three points, while for the fourth point, corresponding to a tail starting time at 50 ns, there is a discrepancy of 5% between the two values. We believe that the difference in this case is due to the uncertainty in the determination of the offset in the direct measurement.

A final comparison is carried out in table III, where we report, for the four different tail starting times for which the direct measurements have been performed, the value of the D parameter and of the mean value of the charge ratio distributions obtained via Monte Carlo and experimentally. The errors on the determination of the mean value have not been reported because they are very small, of the order of 0.001.

This table is a further, final confirmation of the very good agreement between the experimental data and the Monte Carlo results.

Hence we can conclude that through a careful modeling, properly taking into account the detail of the PMT behavior, a faithful description of the PSD capability of a scintillator can be obtained.

It must be stressed, however, that even the approximated analytical procedure, giving results not too different from the Monte Carlo predictions, can be considered good enough to estimate the PSD properties of scintillation cocktails, and it is surely useful to perform at least relative estimates of the discrimination capability of different mixtures.

8. Conclusion

The main outcome of this work is that the characterizations of the PSD properties of liquid scintillators carried out with two different techniques give very consistent estimates. In particular it has been shown that, taking into account properly the PMT characteristics, it is possible to reproduce with a high degree of accuracy, through a complete Monte Carlo modeling having as input the measured waverforms of the scintillation light, the PSD performances obtained in the direct processing of pulses excited in the scintillator by α and β particles. Furthermore, it has been also shown how to choice the processing parameters to optimize the discrimination capability achievable.

Acknowledgments

The authors would like to thank A. Bright for the construction of the experimental set-ups and for the assistance during the measurements.

References

[1] F. D. Brooks, Nucl. Instr. and Meth. 4 (1959) 151.

[2] M. L. Roush, M. A. Wilson and W.F. Hornyak, Nucl. Instr. and Meth. 31 (1964) 112.

[3] F. Frontera et al., Nucl. Instr. and Meth. A 324 (1993) 589.

[4] C. Bacci et al., Phys. Lett. B 293 (1992) 460.

[5] Borexino at Gran Sasso - Proposal for a real time detector for low energy solar neutrinos, eds G. Bellini, M, Campanella and D. Giugni, Dept. of Physics of the Universitity of Milano, INFN - Milano, via Celoria 16 - 20133 Milano, Italy; R.S. Raghavan, AT&T Bell Laboratories, Murray Hill, NJ, USA.

[6] L.M. Bollinger and G.E. Thomas, Rev. Sci. Instr. 32 (1961) 1044.

[7] Y. Koechlin, Thesis, University of Paris (1961).

[8] M.L. Roush, M.A. Wilson and W.F. Hornyak, Nucl. Instr. and Meth. 31 (1964) 112.

[9] G.F. Knoll, Radiation Detection and Measurement, 2nd ed. (Wiley, New York, 1989).

[10] G. Ranucci, Nucl. Instr. and Meth. A 354 (1995) 389.

[11] E. Gatti and F. De Martini, Nuclear Electronics 2, IAEA Wien, (1962) 265.

[12] B. Sabbah and A. Suhami, Nucl. Instr. and Meth. 58 (1968) 102.

[13] G. Ranucci et Al., Nucl. Instr. and Meth. A 350 (1994) 338.

[14] J.B. Birks, The Theory and Practice of Scintillation Counting (Pergamon, Oxford, 1964).

[15] F.J. Lynch, IEEE Trans. Nucl. Sci. NS-22 (1975) 58.

[16] N.H. Clinthorne et al., IEEE Trans. Nucl. Sci. NS-37 (1990) 658

[17] G. Ranucci and Anna Preda, Nucl. Instr. and Meth. A 370 (1996) 597

Figure captions

Figure 1. Effect of oxygen removal through nitrogen flushing on the average light profile. It is evident the relative increase of the amount of light in the tail obtained with longer flushing periods.

Figure 2. Waveshape of the light pulses obtained in a PC+PPO (1.5 g/l) mixture under α and β irradiation.

Figure 3. Waveshape of the light pulses obtained in a PC+PPO (6 g/l) mixture under α and β irradiation.

Figure 4. Waveshape of the light pulses obtained irradiating with α and β particles a sample of the standard scintillator NE213, optimized for pulse shape discrimination

Figure 5. Probability distributions of the fraction of photoelectrons in the tail for α and β pulses, evaluated for 500 ns of integration time and a starting point of the tail at 25 ns after the beginning of the pulse, and for pulse height of 100 photoelectrons. The degree of overlap of the two distributions is the indication of the discrimination achievable.

Figure 6. Plot of the factor of merit D for the PC+PPO (1.5 g/l) scintillator, as function of the beginning of the tail, for various integration times and for a pulse height of 100 photoelectrons. It can be derived that the optimum separation is obtained for the tail starting at 20 ns.

Figure 7. Plot of the factor of merit D for the PC+PPO (6 g/l) scintillator, as function of the beginning of the tail, for various integration times and for a pulse height of 100 photoelectrons. It can be inferred that the optimum separation is obtained for the tail starting at 14 ns.

Figure 8. Plot of the factor of merit D for the NE213 scintillator, as function of the beginning of the tail, for various integration times and for a pulse height of 100

photoelectrons. It can be concluded that the optimum separation is obtained for the tail starting at 18 ns.

Figure 9. Plot of the factor of merit D for the PC+PPO (1.5 g/l) scintillator, as function of the integration time, for a tail starting at 20 ns and for a pulse height of 100 photoelectrons.

Figure 10. Plot of the factor of merit D for the PC+PPO (1.5 g/l) scintillator, as function of the tail starting time, for various integration gates and for a pulse height of 200 photoelectrons. It can be derived that the optimum separation is obtained for the same beginning of the tail of the case of 100 photoelectrons.

Figure 11. Dependence of the D factor for the PC+PPO (1.5 g/l) scintillator vs. the number of photoelectrons, from which it can be inferred the trend proportional to $\sqrt{N_{pe}}$.

Figure 12. Pulse height distribution (a), single photoelectron response (b) and transit time jitter (c) of the RCA 8850 photomultiplier used for the direct application of the charge method.

Figure 13. Typical waveforms of the anode output pulse for a pulse height of 100 photoelectrons obtained via Monte Carlo

Figure 14. Monte Carlo alpha e beta charge ratio distributions evaluated for the PC+PPO (1.5 g/l) scintillator. The calculation has been performed for 100 photoelectrons, an integration gate of 500 ns, and a start of the tail at 25 ns.

Figure 15. Mean value of the charge ratio distribution for beta and alpha events in the PC+PPO (1.5 g/l) scintillator, evaluated analytically and through the Monte Carlo simulation, reported as function of the beginning of the tail. While the two evaluations differ substantially for early starts of the tail, they tend to coincide for delayed tail definitions.

Figure 16. Monte Carlo evaluation of the D parameter obtained for the PC+PPO (1.5 g/l) scintillator shown as function of the definition of the tail, for different integration gates and for a pulse height of 100 photoelectrons.

Figure 17. Monte Carlo evaluation of the D parameter obtained for the PC+PPO (6 g/l) scintillator shown as function of the definition of the tail, for different integration gates and for a pulse height of 100 photoelectrons.

Figure 18. Monte Carlo evaluation of the D parameter obtained for the NE213 scintillator shown as function of the definition of the tail, for different integration gates and for a pulse height of 100 photoelectrons.

Figure 19. Comparison of the D parameter for the PC+PPO (1.5 g/l) scintillator evaluated via Monte Carlo and analytically.The number of photoelectrons per pulse is 100 and the integration gate is 500 ns. It can be noted that in the Monte Carlo result the optimum value of the tail is longer, and the maximum of the D parameter is lower.

Figure 20. Monte Carlo evaluation of the dependence of the optimum value of the D parameter on the number of photoelectrons for the PC+PPO (1.5 g/l). For comparison it is reported also the same plot of figure 11 obtained with the approximated analytical procedure.

Figure 21. Experimental test set-up for the direct characterization of the PSD properties of liquid scintillator samples.

Figure 22. Results of the alpha/beta measurements on the PC+PPO (1.5 g/l) in scatterplot format as function of the number of photoelectrons, together with the projection along the y axis of the interval from 160 to 180 photoelectrons. The measurements have been carried out for an integration gate of 500 ns and for a tail starting at 20 ns

Figure 23. Results of the alpha/beta measurements on the NE213 in scatterplot format as function of the number of photoelectrons, together with the projection along the y

axis of the interval from 160 to 180 photoelectrons. The measurements have been carried out for an integration gate of 500 ns and for a tail starting at 20 ns

Figure 24. D parameter for the PC+PPO (1.5 g/l) scintillator evaluated with the direct method, as function of the beginning of the tail, for different integration gates, and for a pulse height comprised between 160 and 180 photoelectrons

Figure 25. D parameter for the NE213 scintillator evaluated with the direct method, as function of the beginning of the tail, for different integration gates, and for a pulse height comprised between 160 and 180 photoelectrons

Figure 26. Comparison of the experimental distributions of the α and β charge ratios for the PC+PPO (1.5 g/l) scintillator evaluated experimentally and via Monte Carlo. The agreement between them is excellent.

Figure 27. Monte Carlo evaluation and experimental determination of the D parameter for the PC+PPO (1.5 g/l) scintillator. There is a good agreement for the first three points and only a small deviation of 5% for the point evaluated with a tail starting time of 50 ns.

Table I. Parameters of the scintillation pulses produced by beta particles

	τ_1	τ_2	τ_3	q_1	q_2	q_3
PC+PPO (1.5 g/l)	3.57	17.61	59.50	0.895	0.063	0.042
PC+PPO (6 g/l)	1.75	8.12	71.25	0.856	0.131	0.013
Ne213	3.86	24.28	73.62	0.912	0.045	0.043

Table II. Parameters of the scintillation pulses produced by alpha particles

	τ_1	τ_2	τ_3	τ_4	q_1	q_2	q_3	q_4
PC+PPO (1.5 g/l)	3.25	13.49	59.95	279.10	0.630	0.178	0.119	0.073
PC+PPO (6 g/l)	2.03	13.10	56.19	399.60	0.625	0.162	0.108	0.105
Ne213	3.89	20.60	92.36	440.0	0.470	0.223	0.191	0.116

Table III. Comparison of the D factors of merit and of the mean values of the charge ratio distribution for the PC+PPO (1.5 g/l) scintillator, evaluated experimentally and via Monte Carlo for four different tail definitions.

Start of the tail	D		Mean value			
	Monte Carlo	Experimental data	Alpha		Beta	
			M.C.	Ex. data	M.C.	Ex. data
20	3.02 ± 0.07	3.06 ± 0.07	0.359	0.377	0.236	0.238
25	3.27 ± 0.07	3.24 ± 0.07	0.268	0.289	0.140	0.148
30	3.24 ± 0.07	3.21 ± 0.07	0.201	0.236	0.076	0.103
50	2.79±0.07	2.94±0.07	0.118	0.148	0.0251	0.035

FIGURE 1

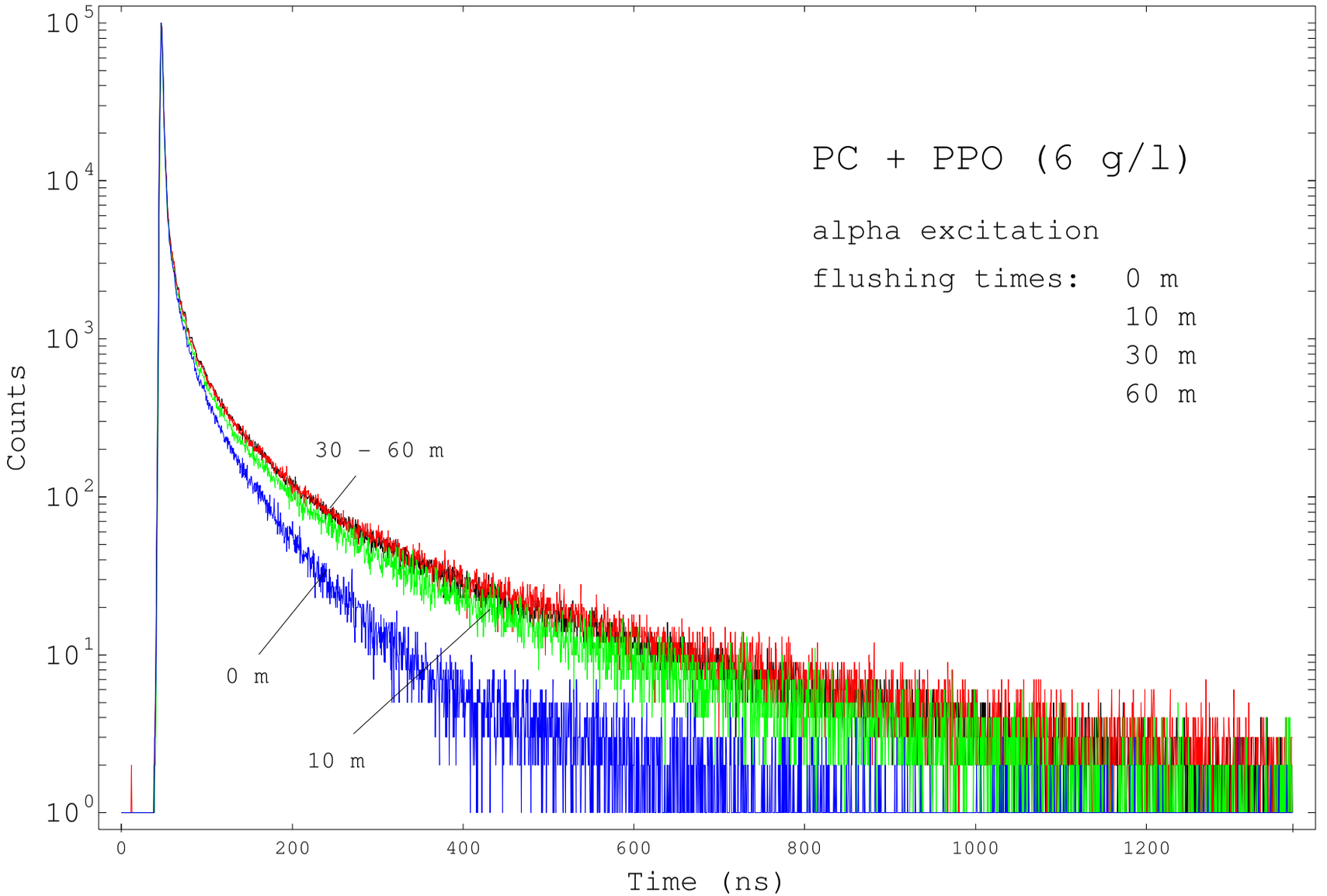
PC + PPO (6 g/l)
alpha excitation
flushing times: 0 m
10 m
30 m
60 m
30 – 60 m
0 m
10 m
Counts
Time (ns)
10^0
10^1
10^2
10^3
10^4
10^5
0
200
400
600
800
1000
1200

FIGURE 2

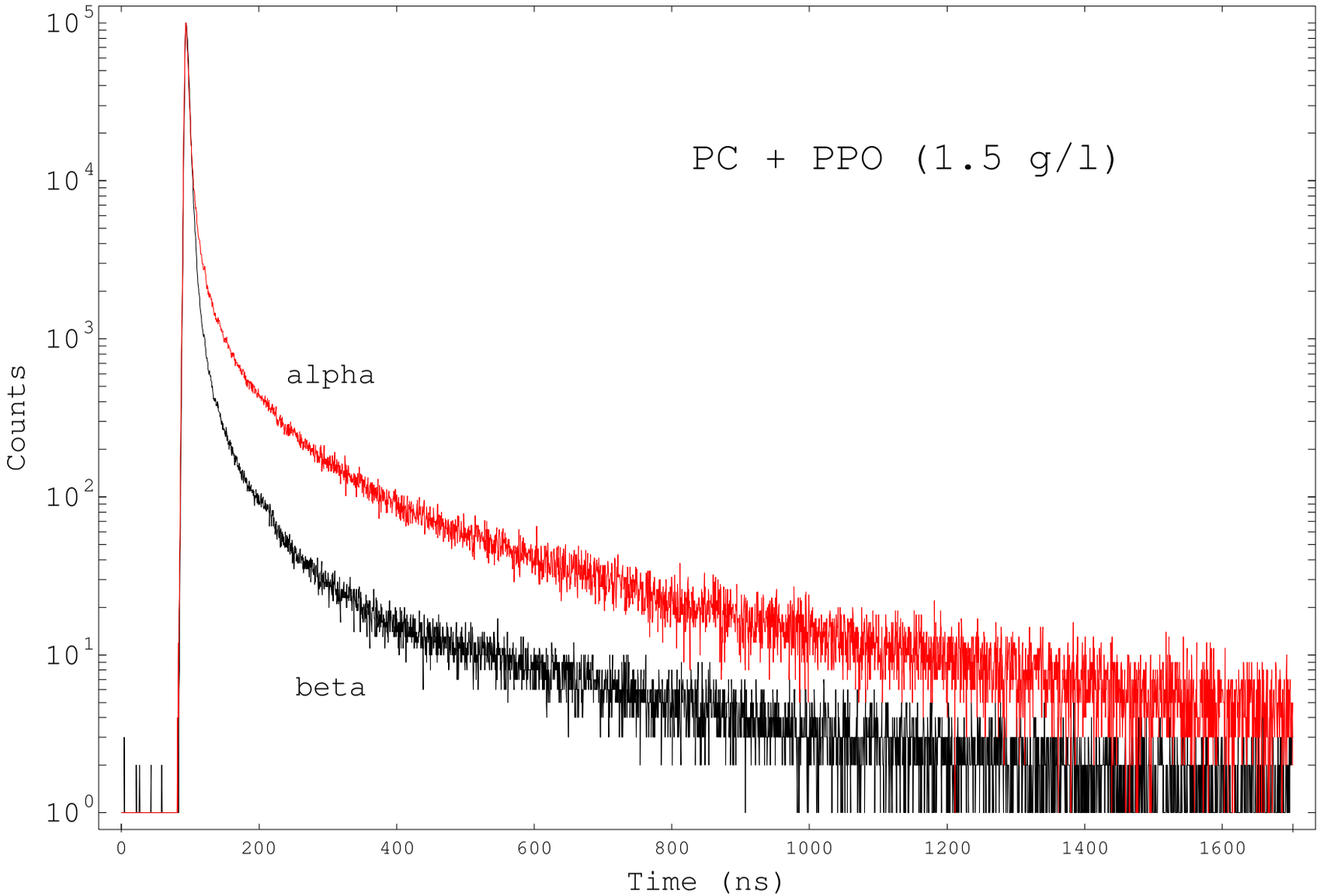
PC + PPO (1.5 g/l)
alpha
beta
Counts
Time (ns)
10^5
10^4
10^3
10^2
10^1
10^0
0
200
400
600
800
1000
1200
1400
1600

FIGURE 3

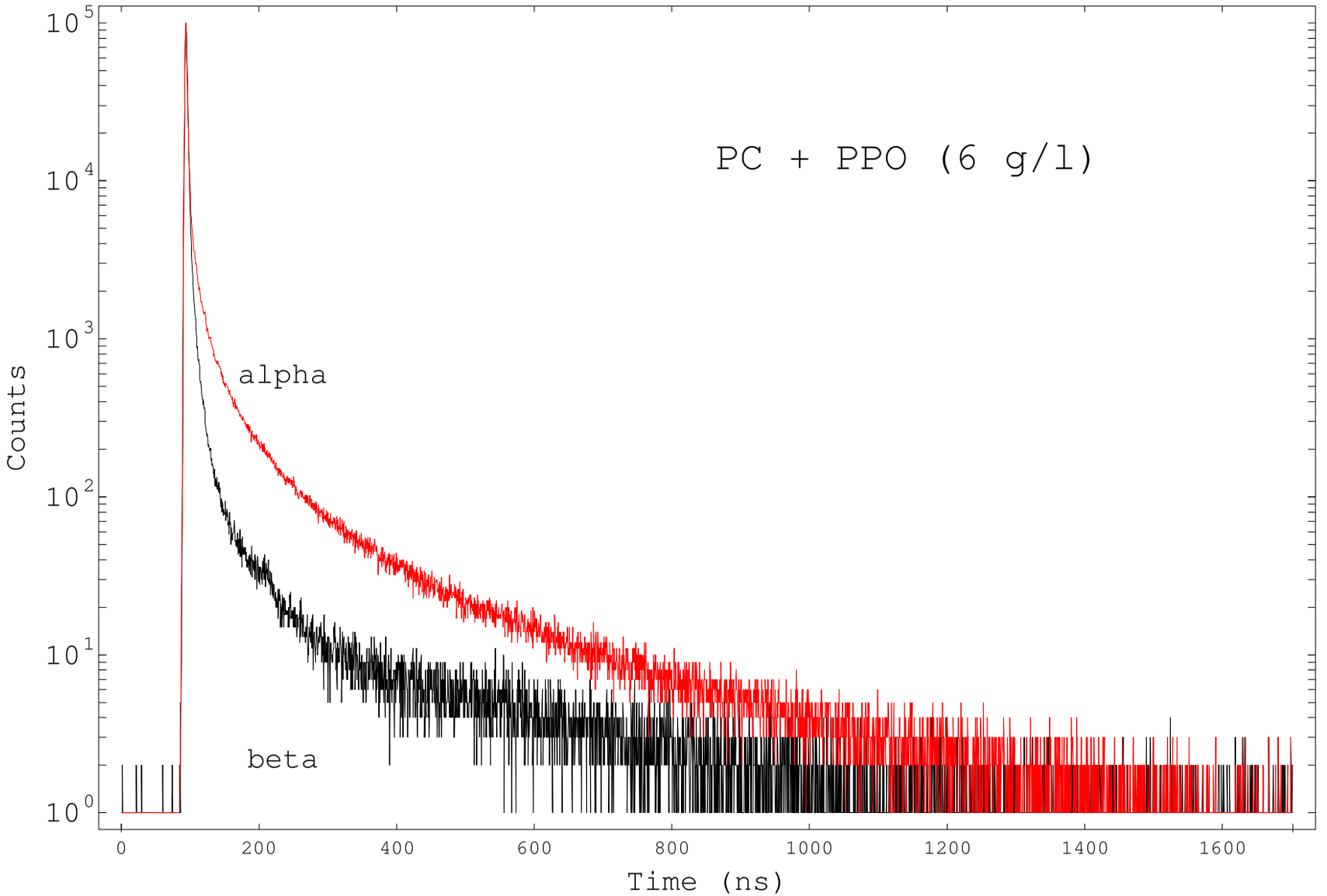
PC + PPO (6 g/l)
alpha
beta
Counts
Time (ns)
10^5
10^4
10^3
10^2
10^1
10^0
0
200
400
600
800
1000
1200
1400
1600

FIGURE 4

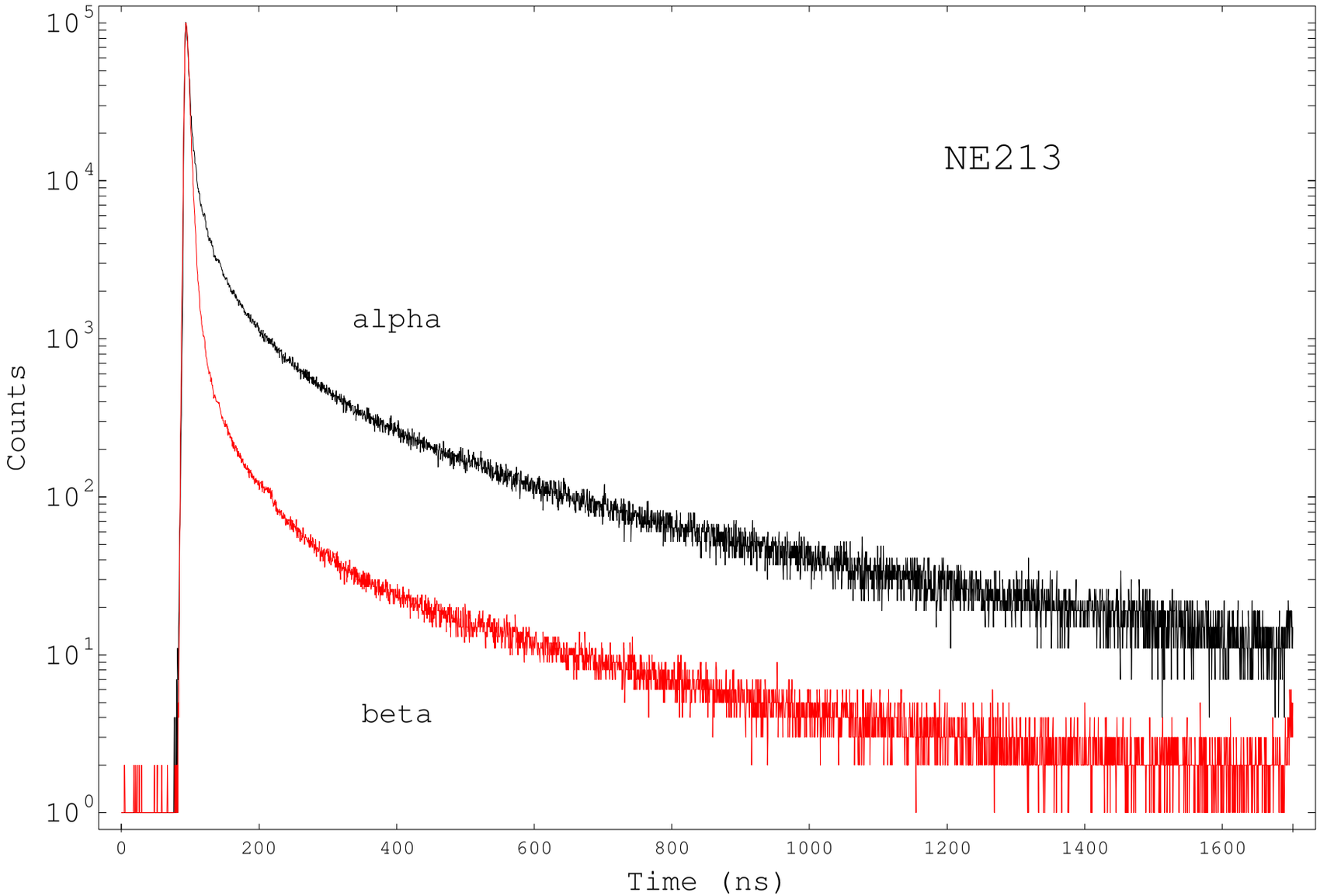
NE213
alpha
beta
Counts
Time (ns)
10^5
10^4
10^3
10^2
10^1
10^0
0
200
400
600
800
1000
1200
1400
1600

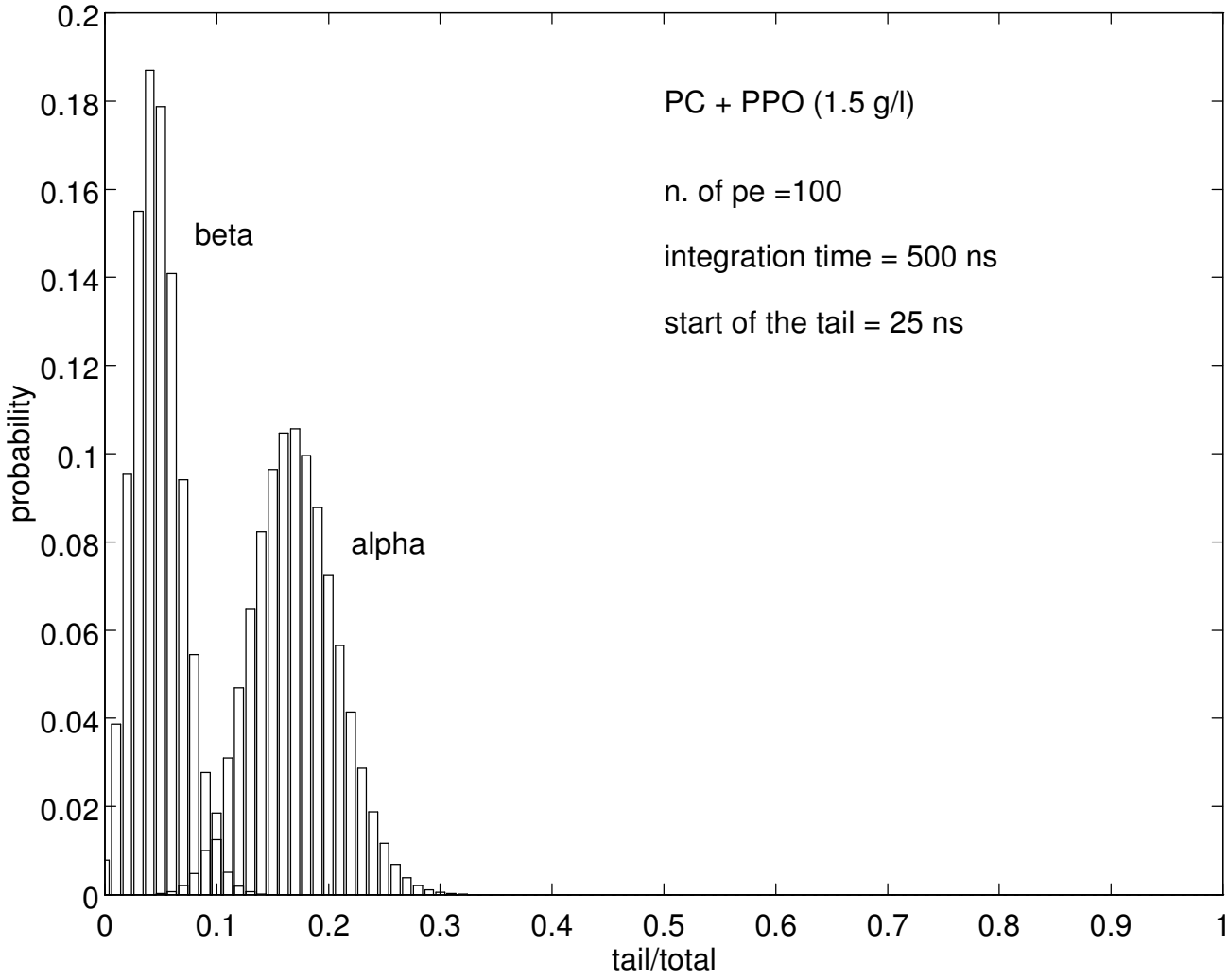
PC + PPO (1.5 g/l)
n. of pe =100
integration time = 500 ns
start of the tail = 25 ns
beta
alpha
probability
tail/total
0
0.02
0.04
0.06
0.08
0.1
0.12
0.14
0.16
0.18
0.2
0.1
0.2
0.3
0.4
0.5
0.6
0.7
0.8
0.9
1

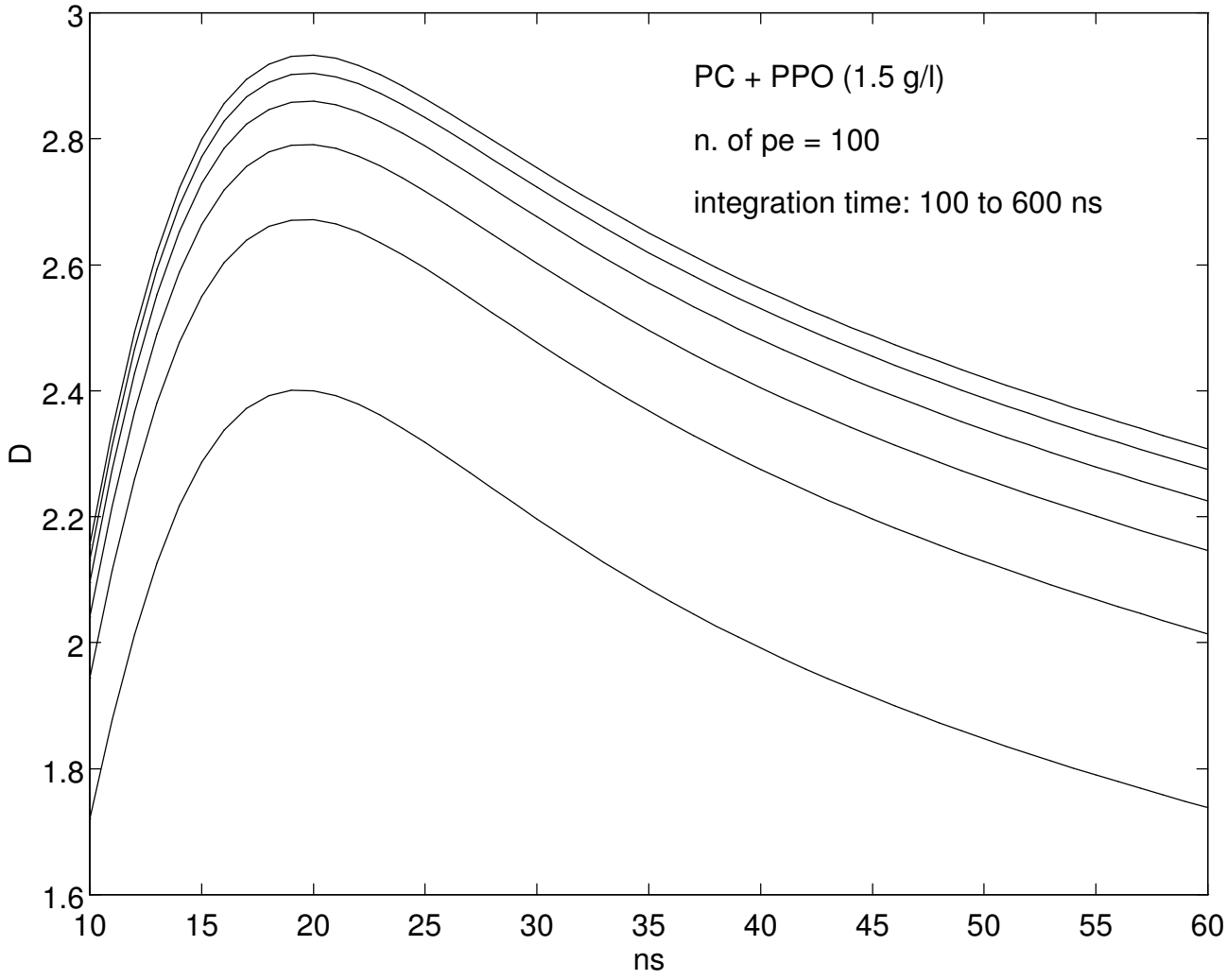
PC + PPO (1.5 g/l)
n. of pe = 100
integration time: 100 to 600 ns
D
ns
3
2.8
2.6
2.4
2.2
2
1.8
1.6
10
15
20
25
30
35
40
45
50
55
60

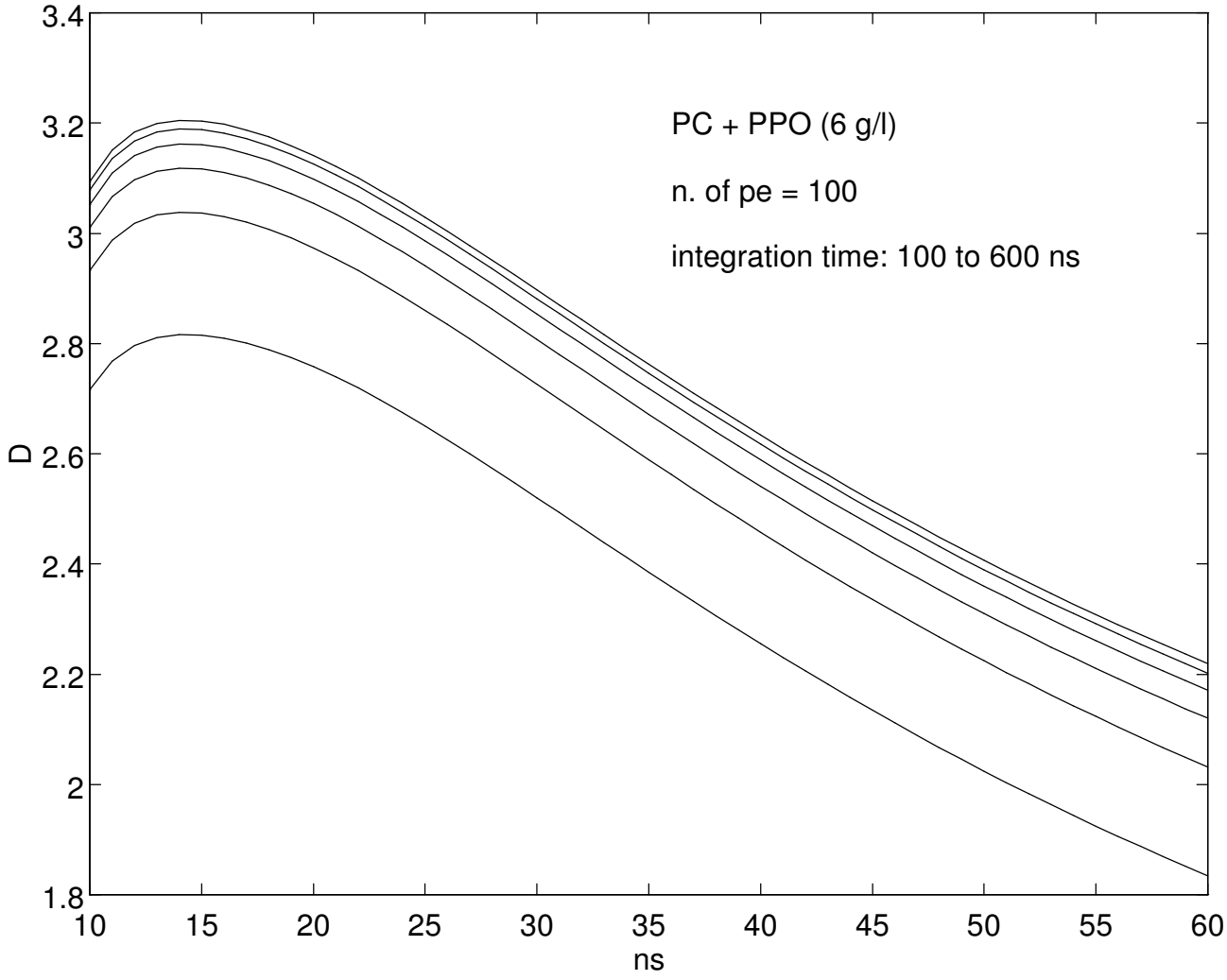
PC + PPO (6 g/l)
n. of pe = 100
integration time: 100 to 600 ns
D
ns
3.4
3.2
3
2.8
2.6
2.4
2.2
2
1.8
10
15
20
25
30
35
40
45
50
55
60

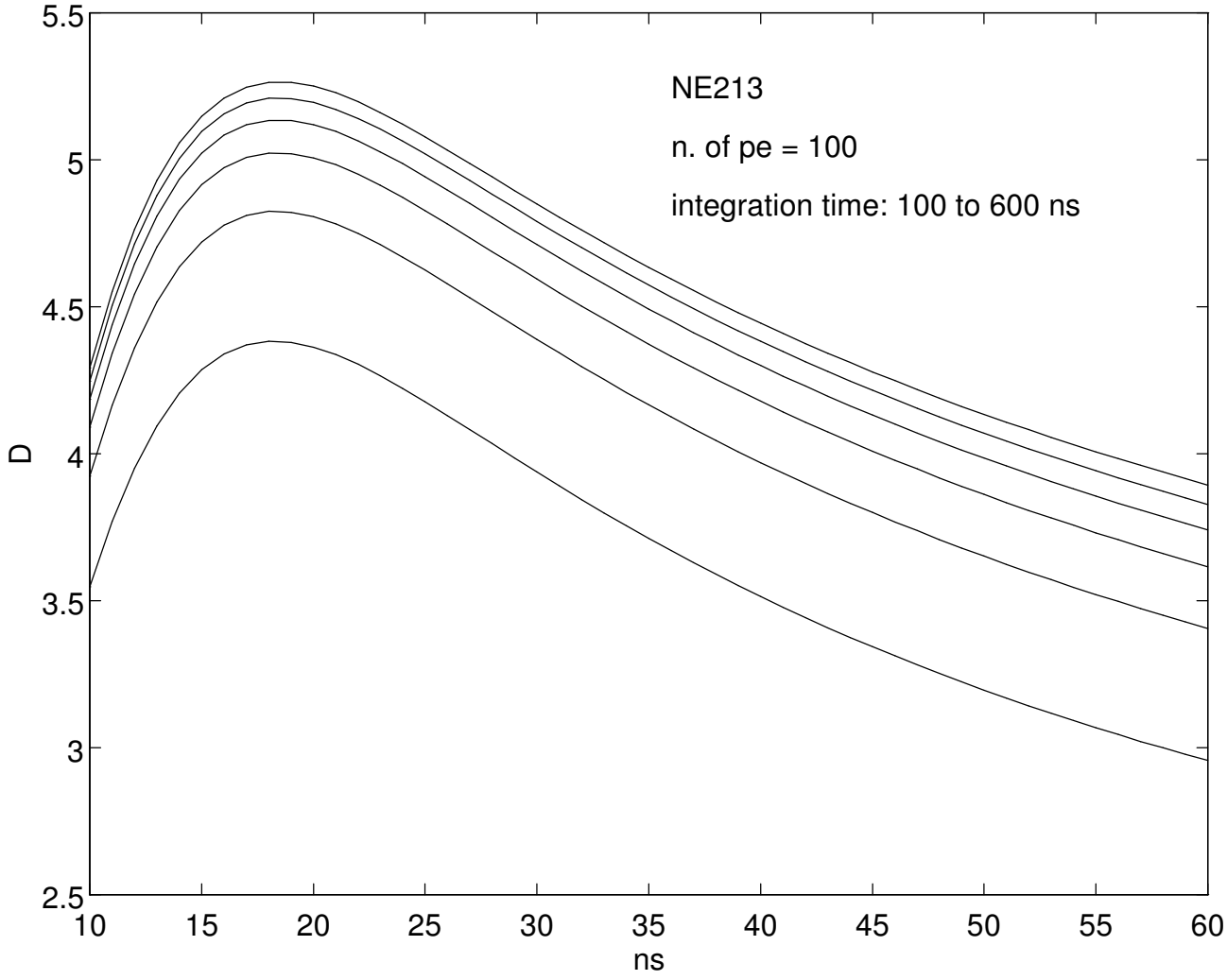
NE213
n. of pe = 100
integration time: 100 to 600 ns
D
ns
5.5
5
4.5
4
3.5
3
2.5
10
15
20
25
30
35
40
45
50
55
60

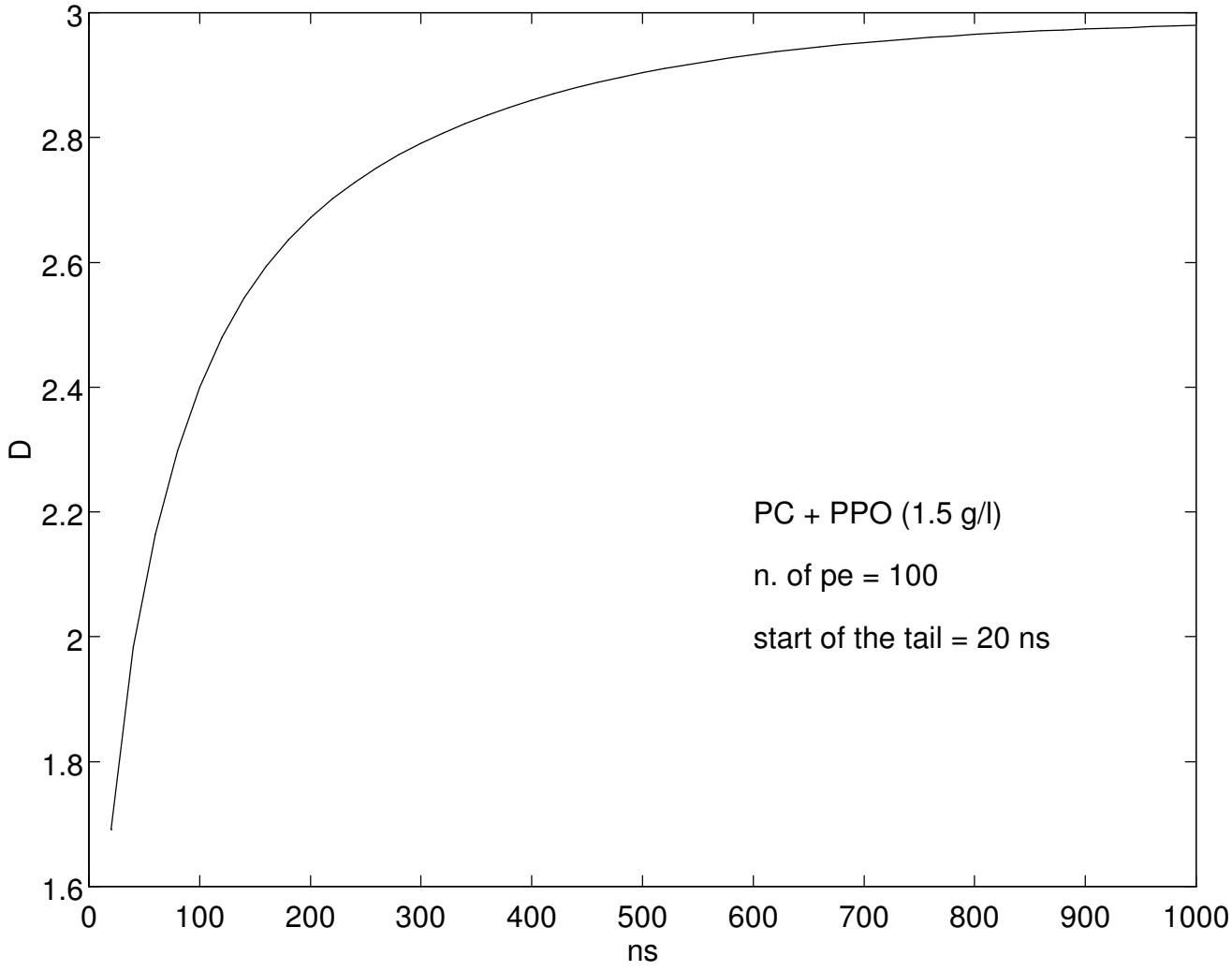
3
2.8
2.6
2.4
2.2
2
1.8
1.6
D
0
100
200
300
400
500
600
700
800
900
1000
ns
PC + PPO (1.5 g/l)
n. of pe = 100
start of the tail = 20 ns

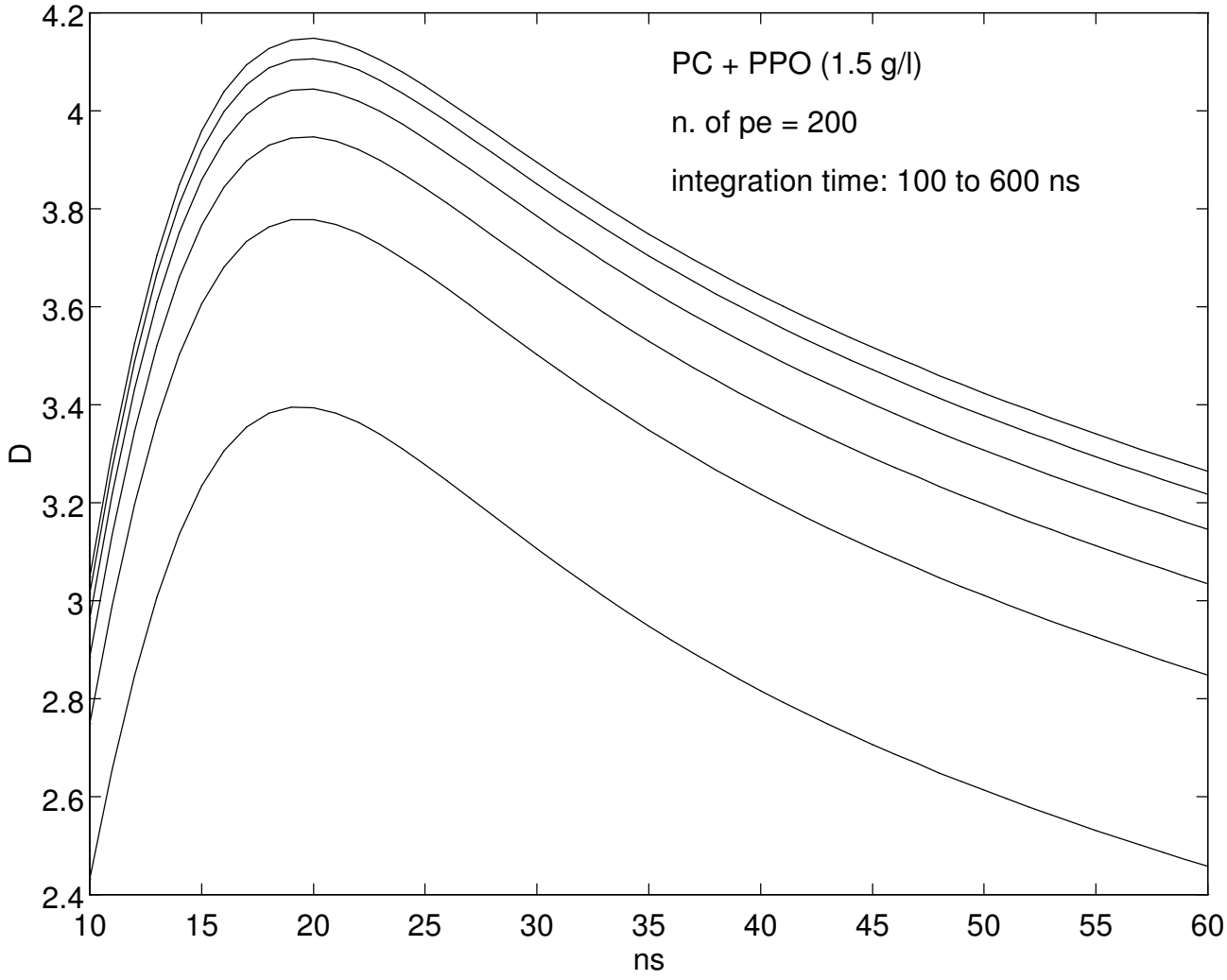
PC + PPO (1.5 g/l)
n. of pe = 200
integration time: 100 to 600 ns
D
ns
4.2
4
3.8
3.6
3.4
3.2
3
2.8
2.6
2.4
10
15
20
25
30
35
40
45
50
55
60

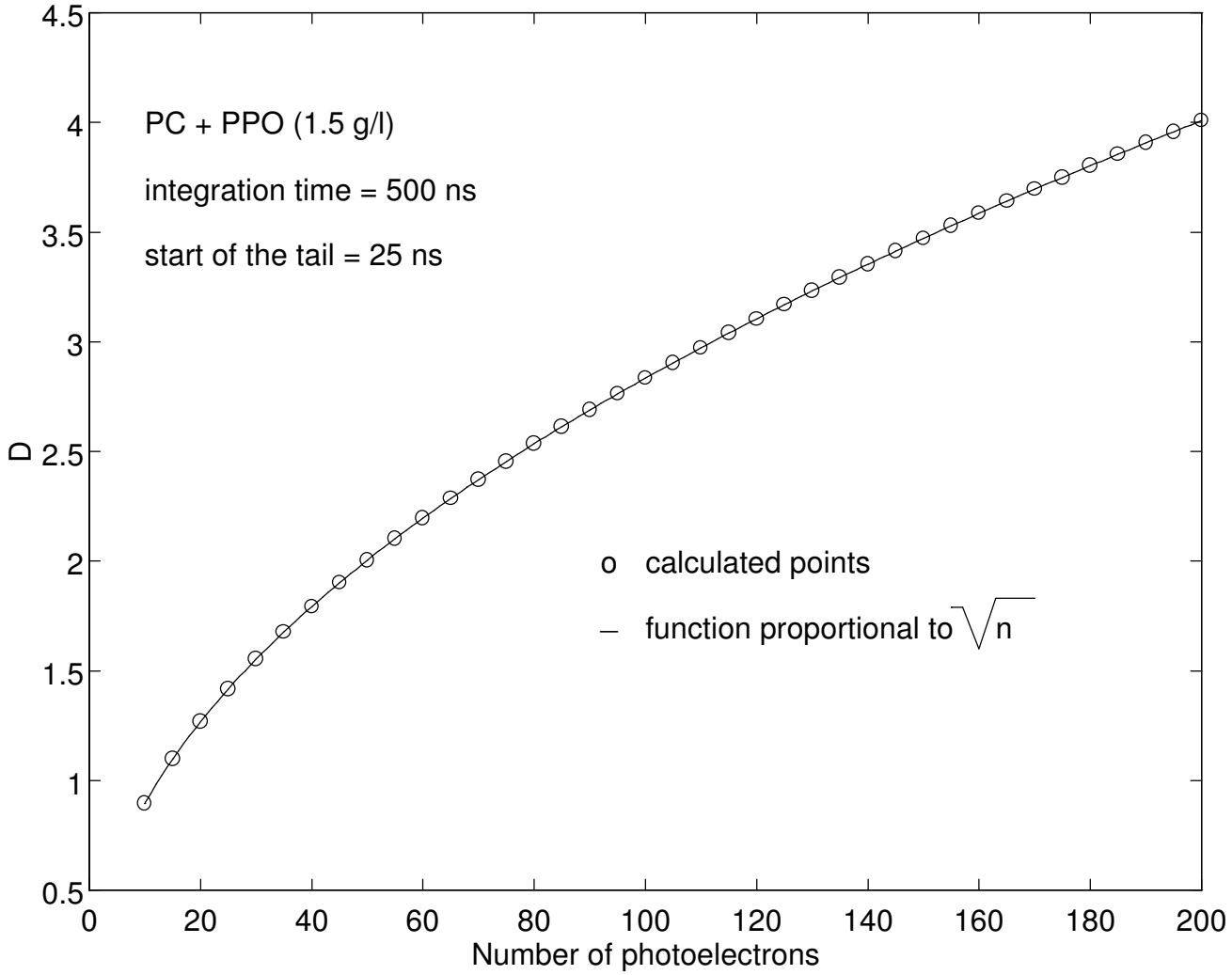
PC + PPO (1.5 g/l)
integration time = 500 ns
start of the tail = 25 ns
o calculated points
– function proportional to √n
D
Number of photoelectrons
4.5
4
3.5
3
2.5
2
1.5
1
0.5
0
20
40
60
80
100
120
140
160
180
200

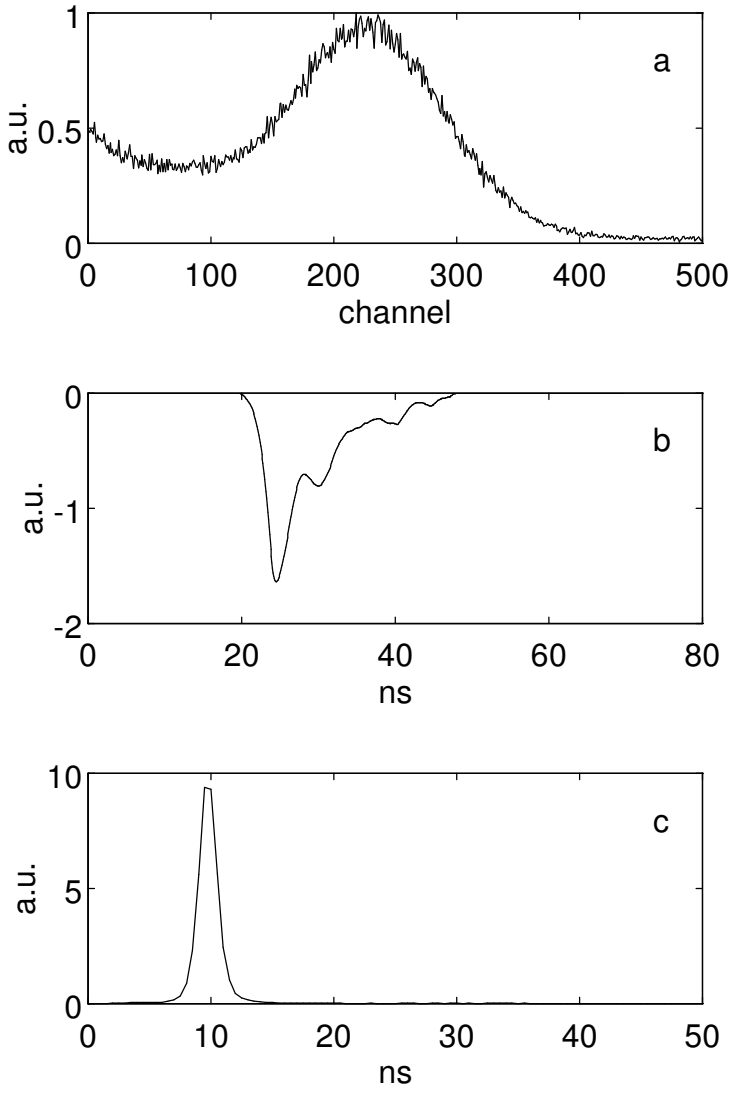
a
a.u.
channel
b
a.u.
ns
c
a.u.
ns

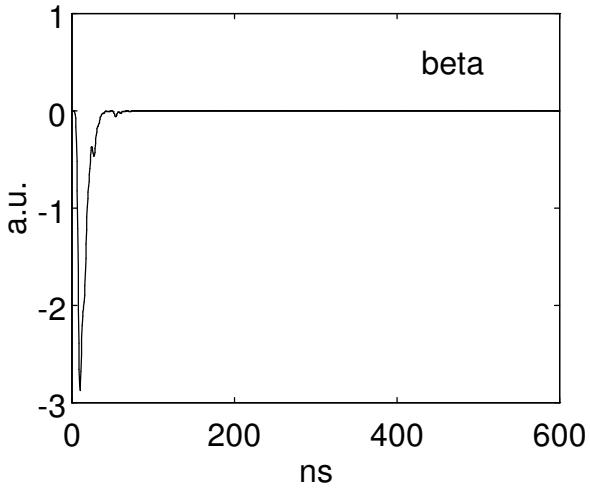
beta
a.u.
1
0
-1
-2
-3
0
200
400
600
ns

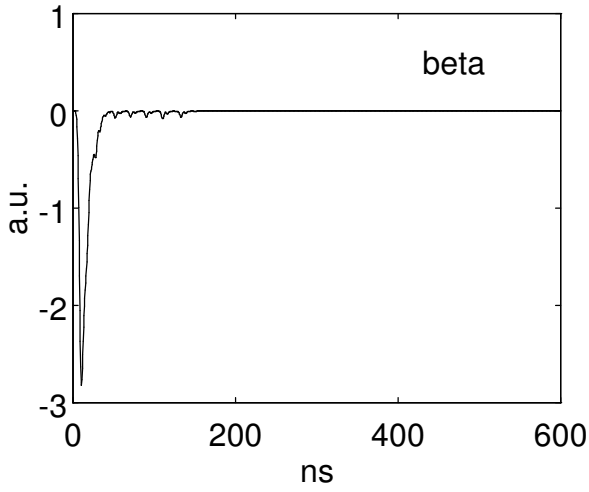
beta
a.u.
1
0
-1
-2
-3
0
200
400
600
ns

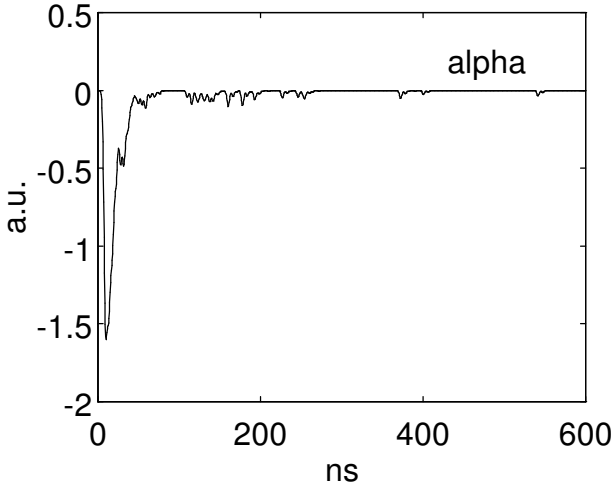
alpha
a.u.
0.5
0
-0.5
-1
-1.5
-2
0
200
400
600
ns

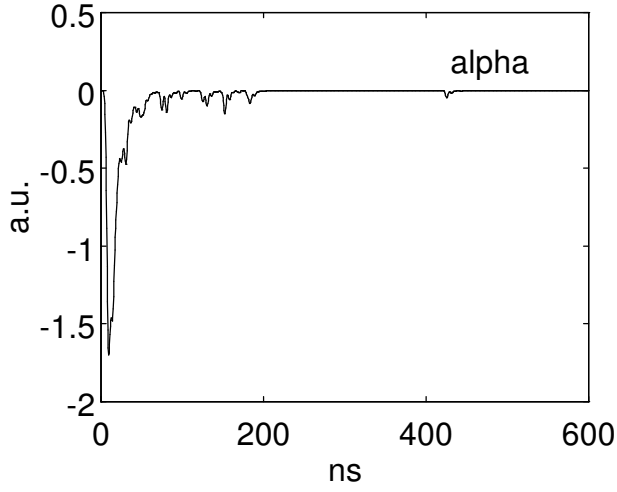
alpha
a.u.
0.5
0
-0.5
-1
-1.5
-2
0
200
400
600
ns

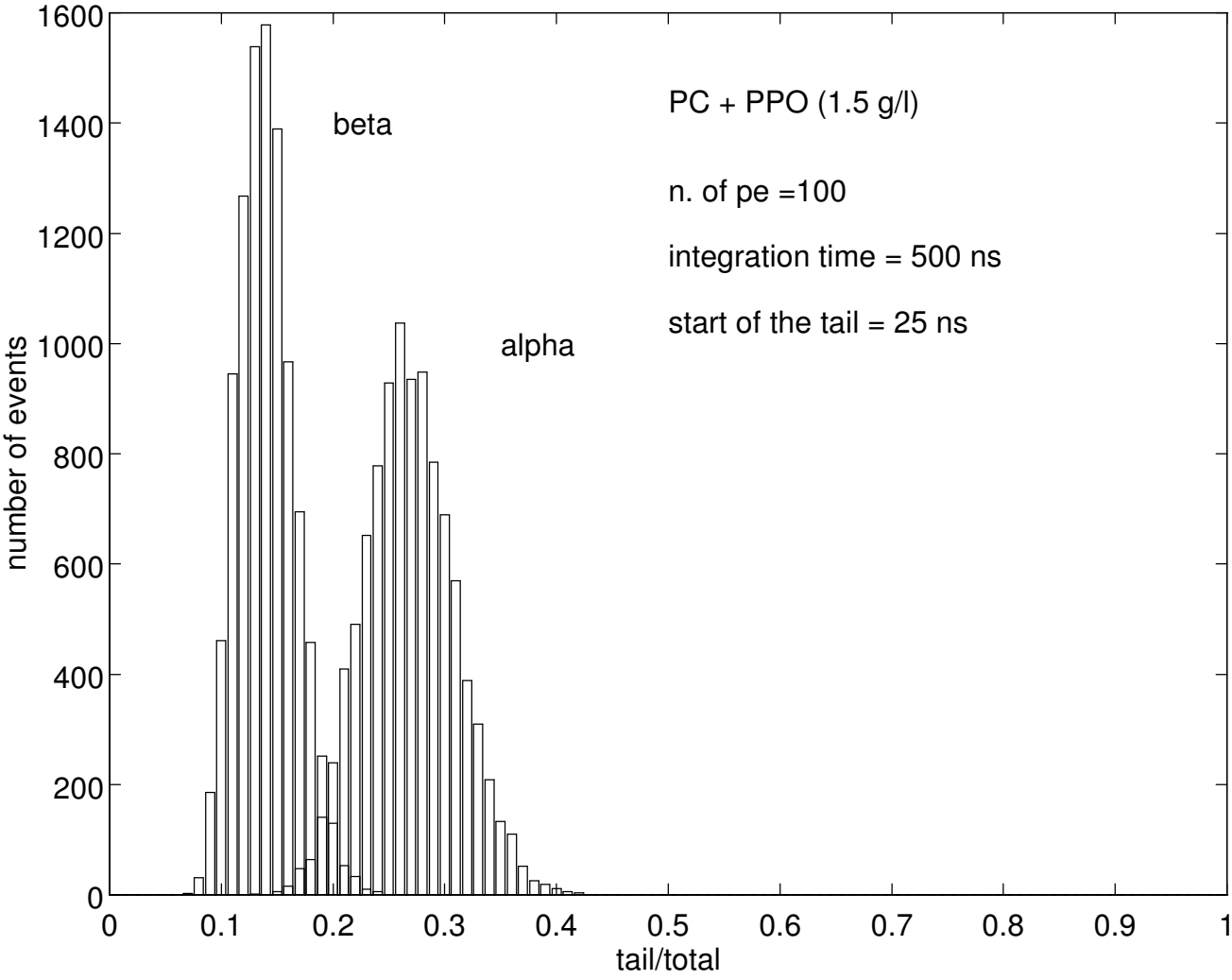
1600
1400
1200
1000
800
600
400
200
0
number of events
0
0.1
0.2
0.3
0.4
0.5
0.6
0.7
0.8
0.9
1
tail/total
beta
alpha
PC + PPO (1.5 g/l)
n. of pe =100
integration time = 500 ns
start of the tail = 25 ns

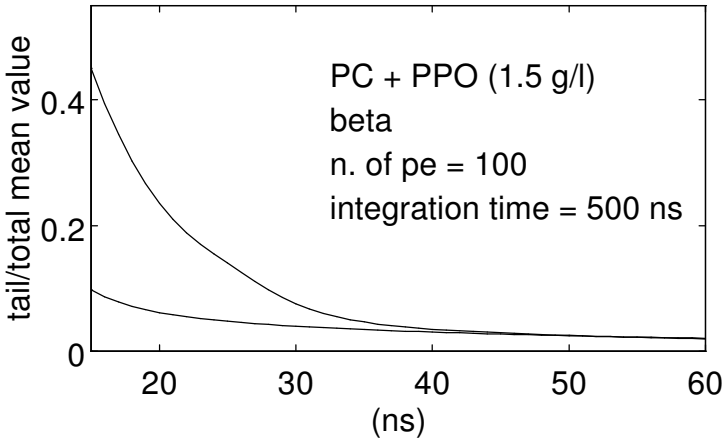
tail/total mean value
0.4
0.2
0
20
30
40
50
60
(ns)
PC + PPO (1.5 g/l)
beta
n. of pe = 100
integration time = 500 ns

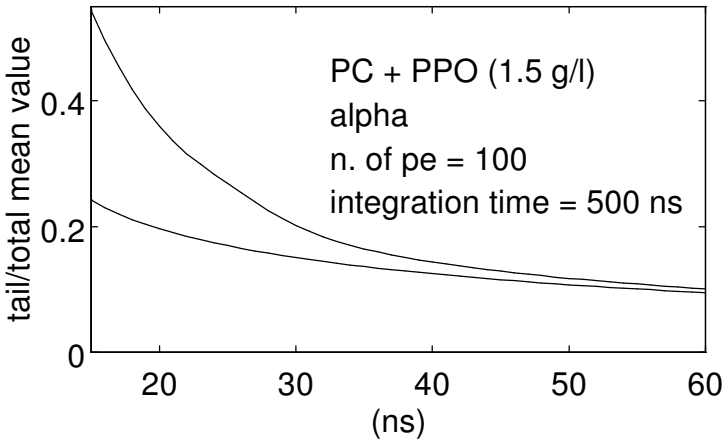
tail/total mean value
0.4
0.2
0
20
30
40
50
60
(ns)
PC + PPO (1.5 g/l)
alpha
n. of pe = 100
integration time = 500 ns

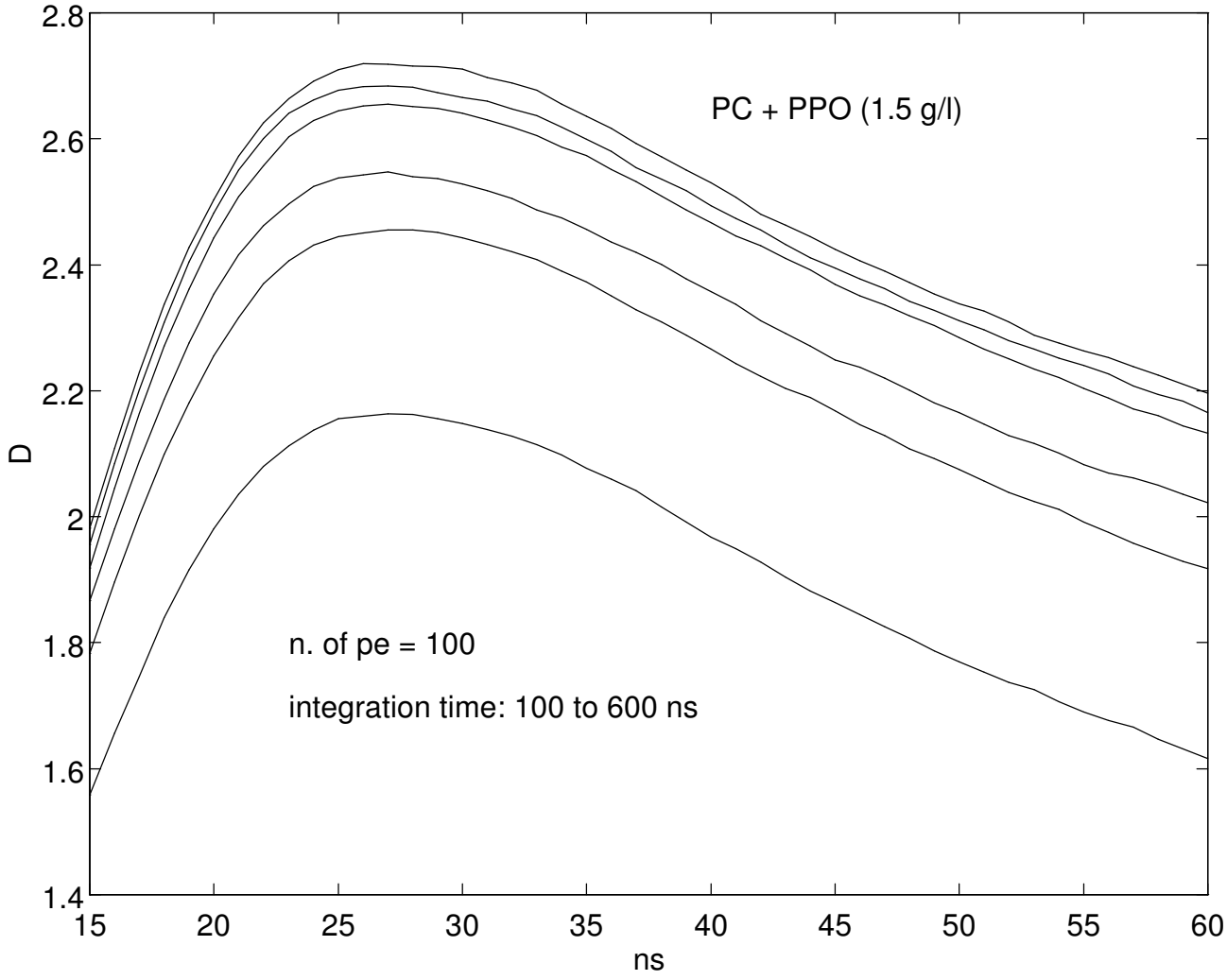
PC + PPO (1.5 g/l)
n. of pe = 100
integration time: 100 to 600 ns
D
ns
2.8
2.6
2.4
2.2
2
1.8
1.6
1.4
15
20
25
30
35
40
45
50
55
60

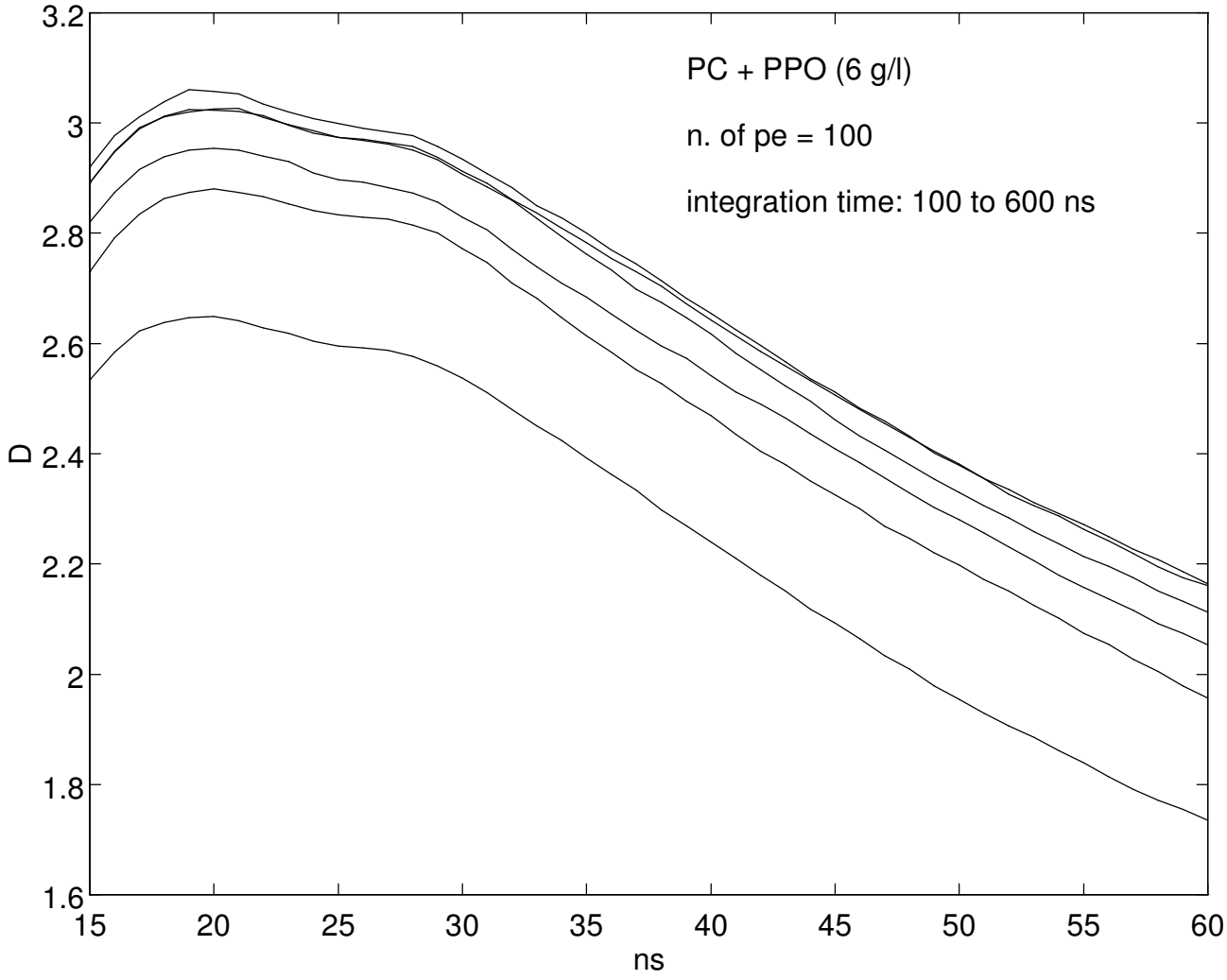
PC + PPO (6 g/l)
n. of pe = 100
integration time: 100 to 600 ns
D
ns
3.2
3
2.8
2.6
2.4
2.2
2
1.8
1.6
15
20
25
30
35
40
45
50
55
60

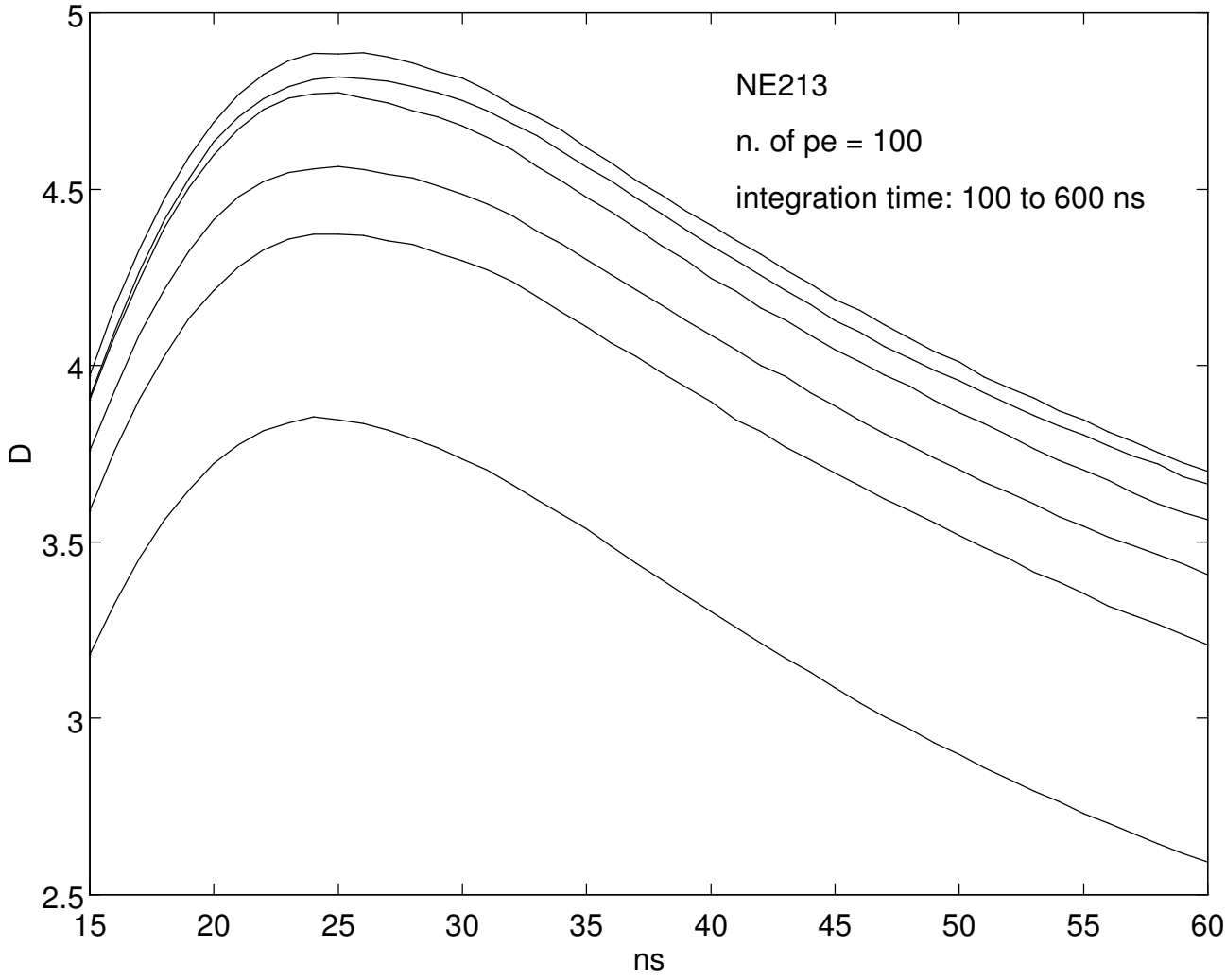
NE213
n. of pe = 100
integration time: 100 to 600 ns
D
ns
5
4.5
4
3.5
3
2.5
15
20
25
30
35
40
45
50
55
60

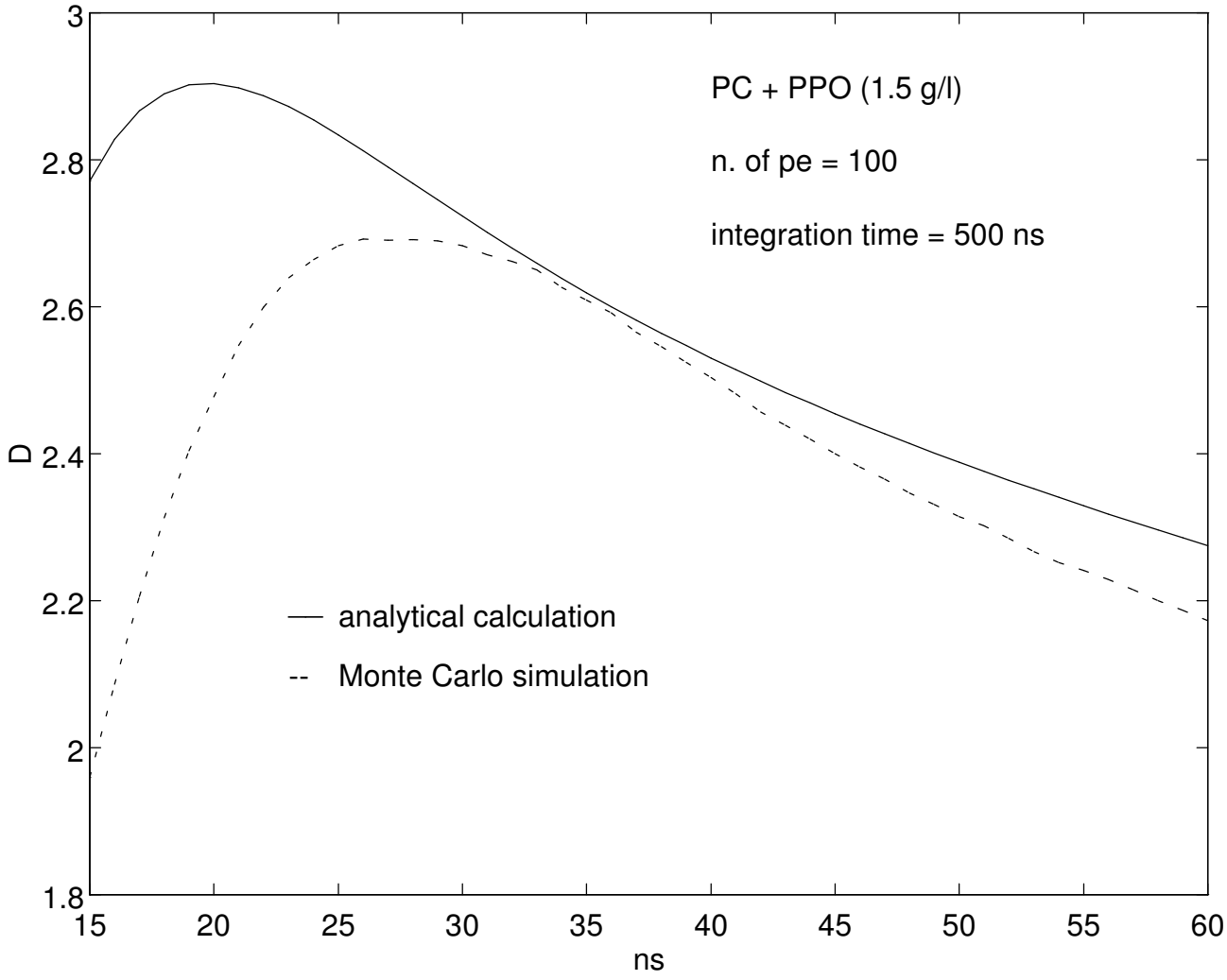
PC + PPO (1.5 g/l)
n. of pe = 100
integration time = 500 ns
analytical calculation
Monte Carlo simulation
D
ns
3
2.8
2.6
2.4
2.2
2
1.8
15
20
25
30
35
40
45
50
55
60

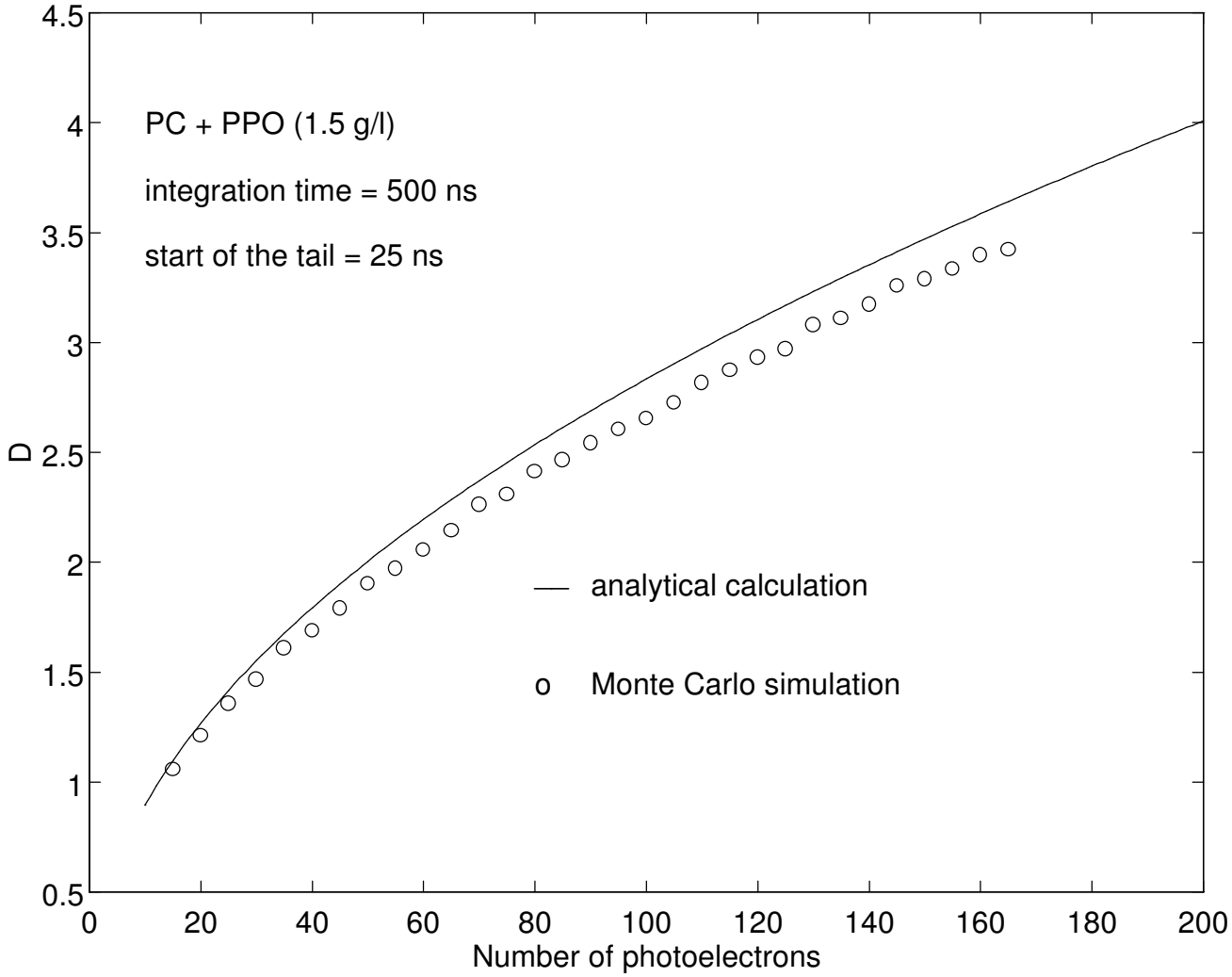
PC + PPO (1.5 g/l)
integration time = 500 ns
start of the tail = 25 ns
analytical calculation
Monte Carlo simulation
D
Number of photoelectrons
4.5
4
3.5
3
2.5
2
1.5
1
0.5
0
20
40
60
80
100
120
140
160
180
200

FIGURE 21

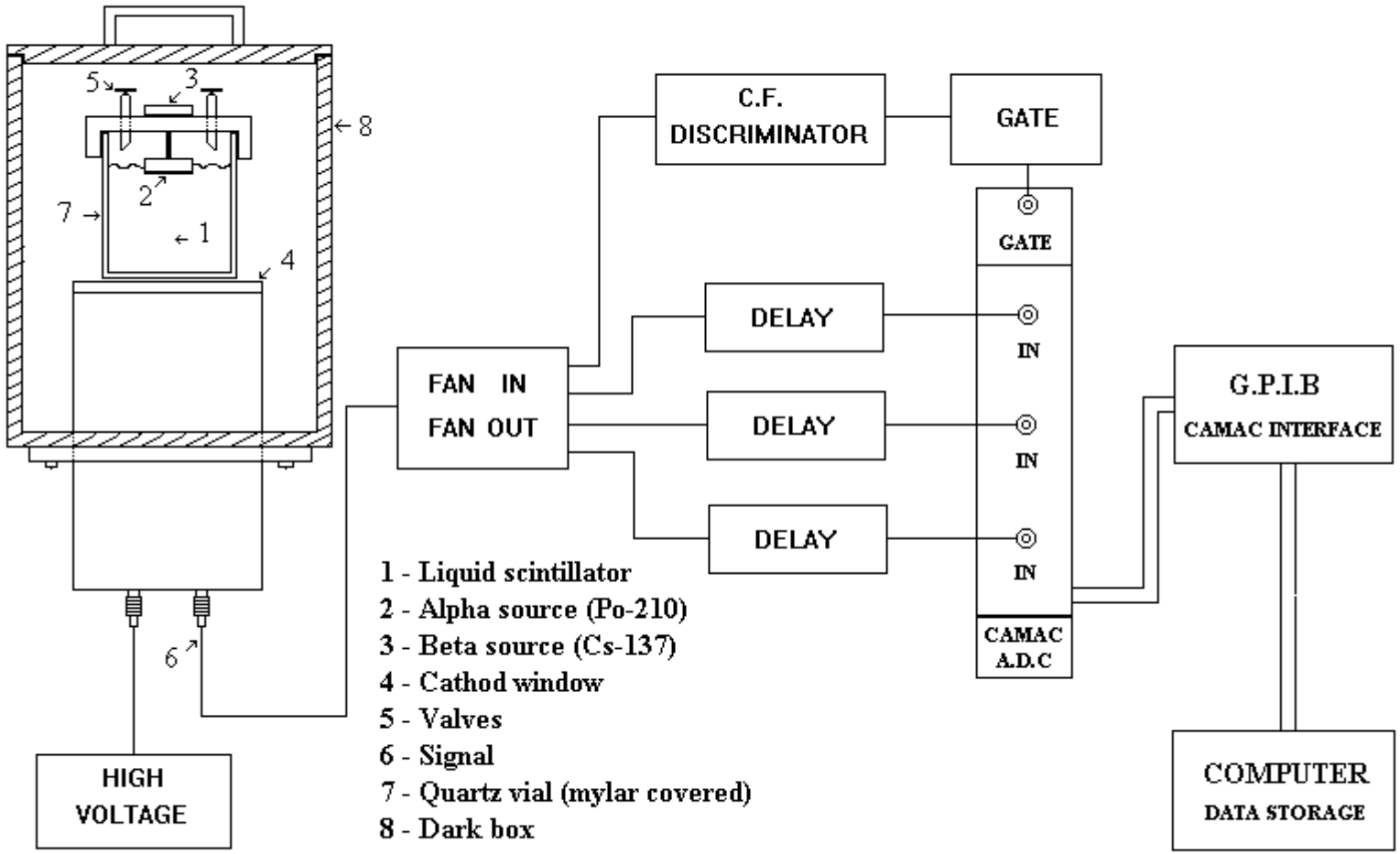
5
3
8
7
2
1
4
6
C.F.
DISCRIMINATOR
GATE
GATE
DELAY
DELAY
DELAY
IN
IN
IN
FAN IN
FAN OUT
CAMAC
A.D.C
G.P.I.B
CAMAC INTERFACE
HIGH
VOLTAGE
COMPUTER
DATA STORAGE
1 - Liquid scintillator
2 - Alpha source (Po-210)
3 - Beta source (Cs-137)
4 - Cathod window
5 - Valves
6 - Signal
7 - Quartz vial (mylar covered)
8 - Dark box

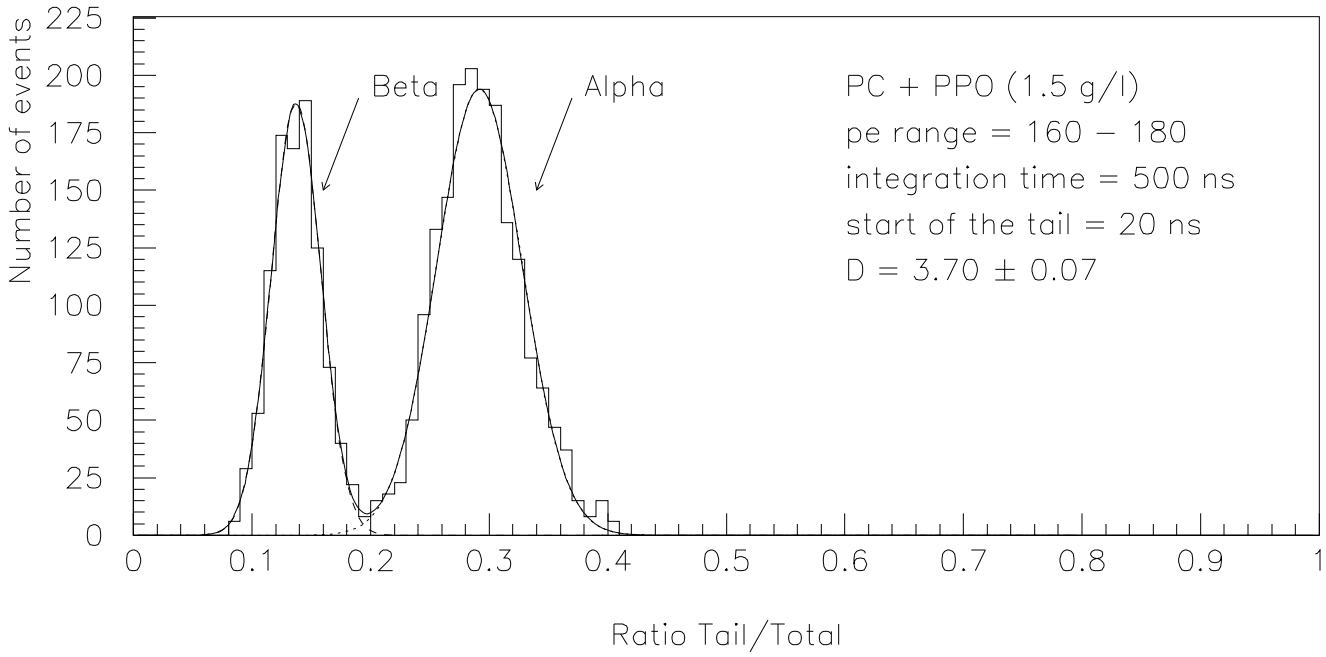
Number of events
225
200
175
150
125
100
75
50
25
0
Beta
Alpha
PC + PPO (1.5 g/l)
pe range = 160 – 180
integration time = 500 ns
start of the tail = 20 ns
D = 3.70 ± 0.07
0
0.1
0.2
0.3
0.4
0.5
0.6
0.7
0.8
0.9
1
Ratio Tail/Total

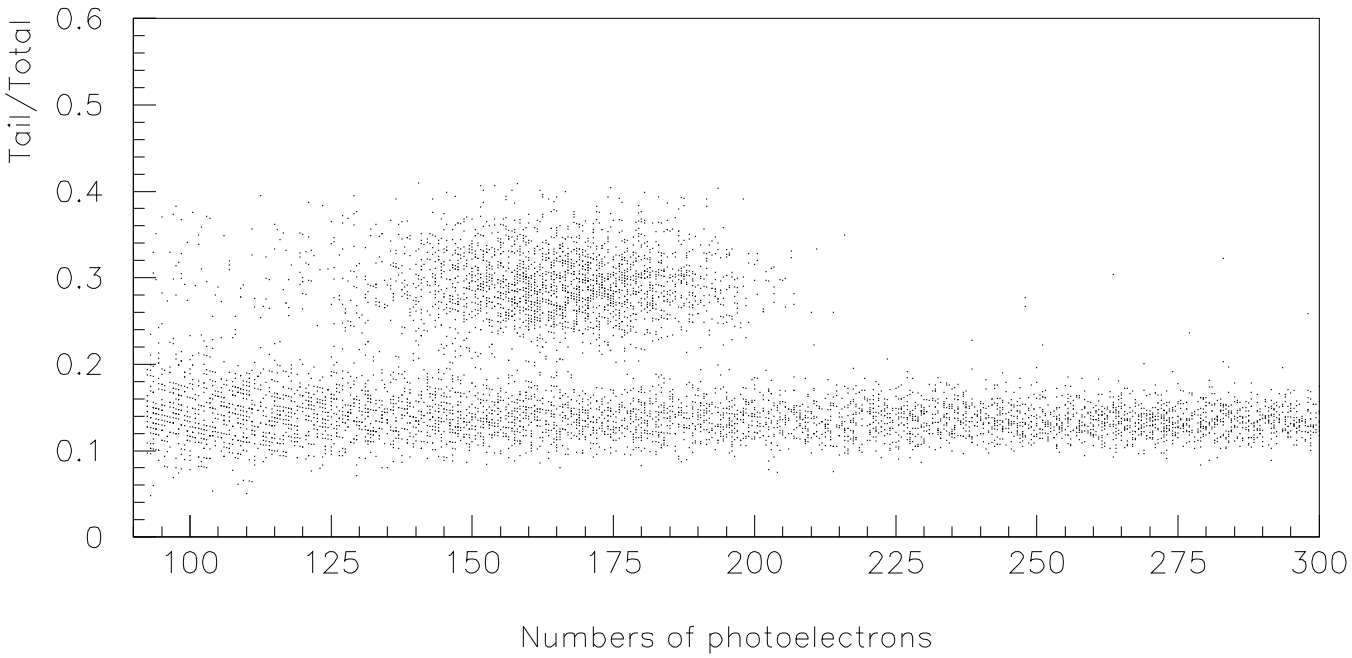
Tail/Total
0.6
0.5
0.4
0.3
0.2
0.1
0
100
125
150
175
200
225
250
275
300
Numbers of photoelectrons

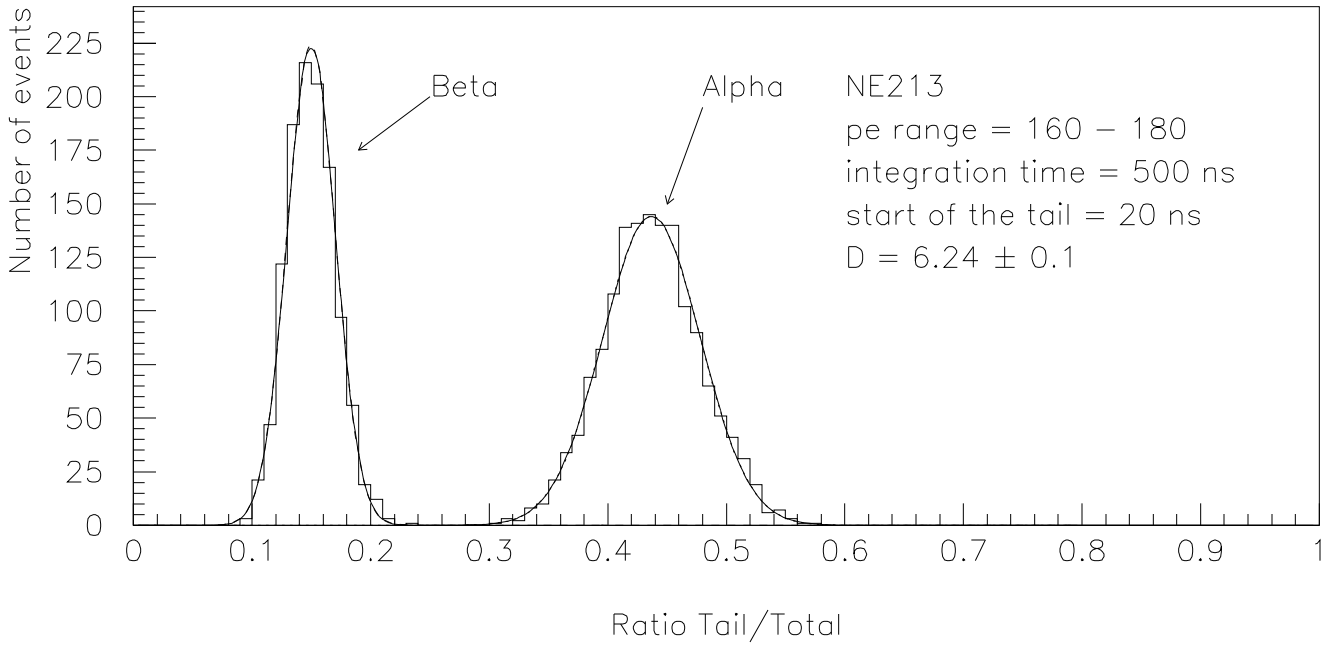
Number of events
225
200
175
150
125
100
75
50
25
0
Beta
Alpha
NE213
pe range = 160 – 180
integration time = 500 ns
start of the tail = 20 ns
D = 6.24 ± 0.1
0
0.1
0.2
0.3
0.4
0.5
0.6
0.7
0.8
0.9
1
Ratio Tail/Total

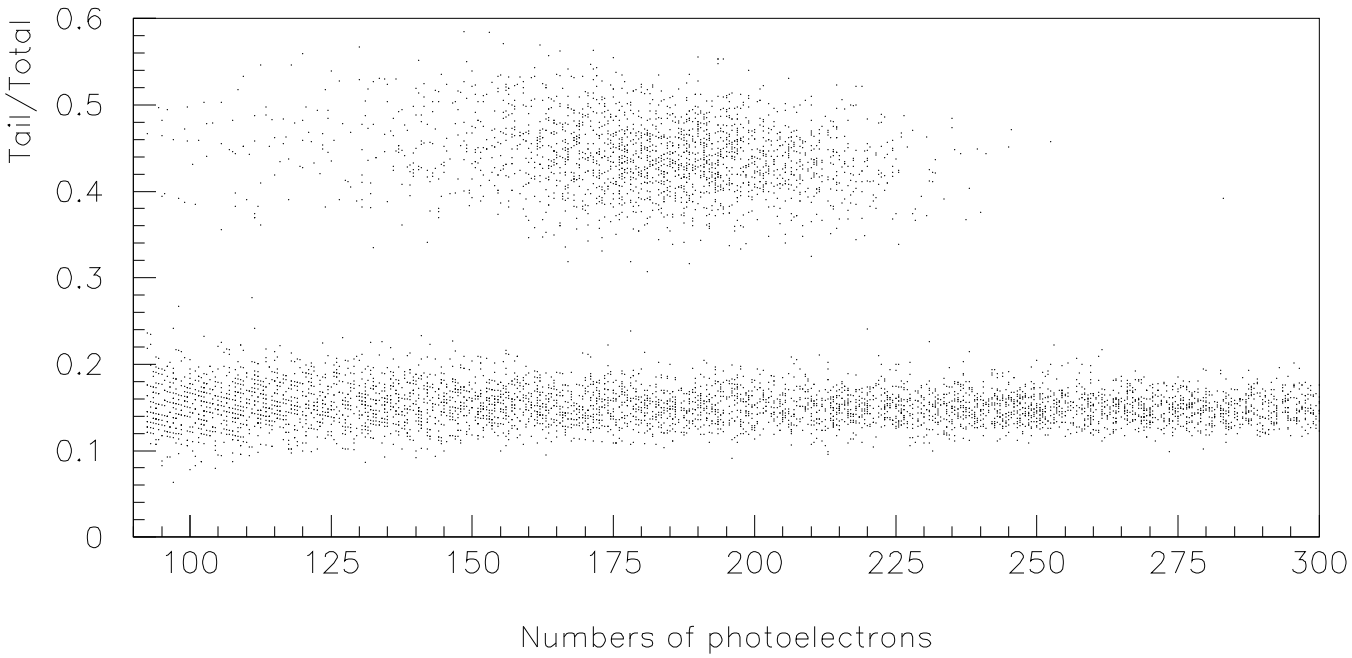
Tail/Total
0.6
0.5
0.4
0.3
0.2
0.1
0
100
125
150
175
200
225
250
275
300
Numbers of photoelectrons

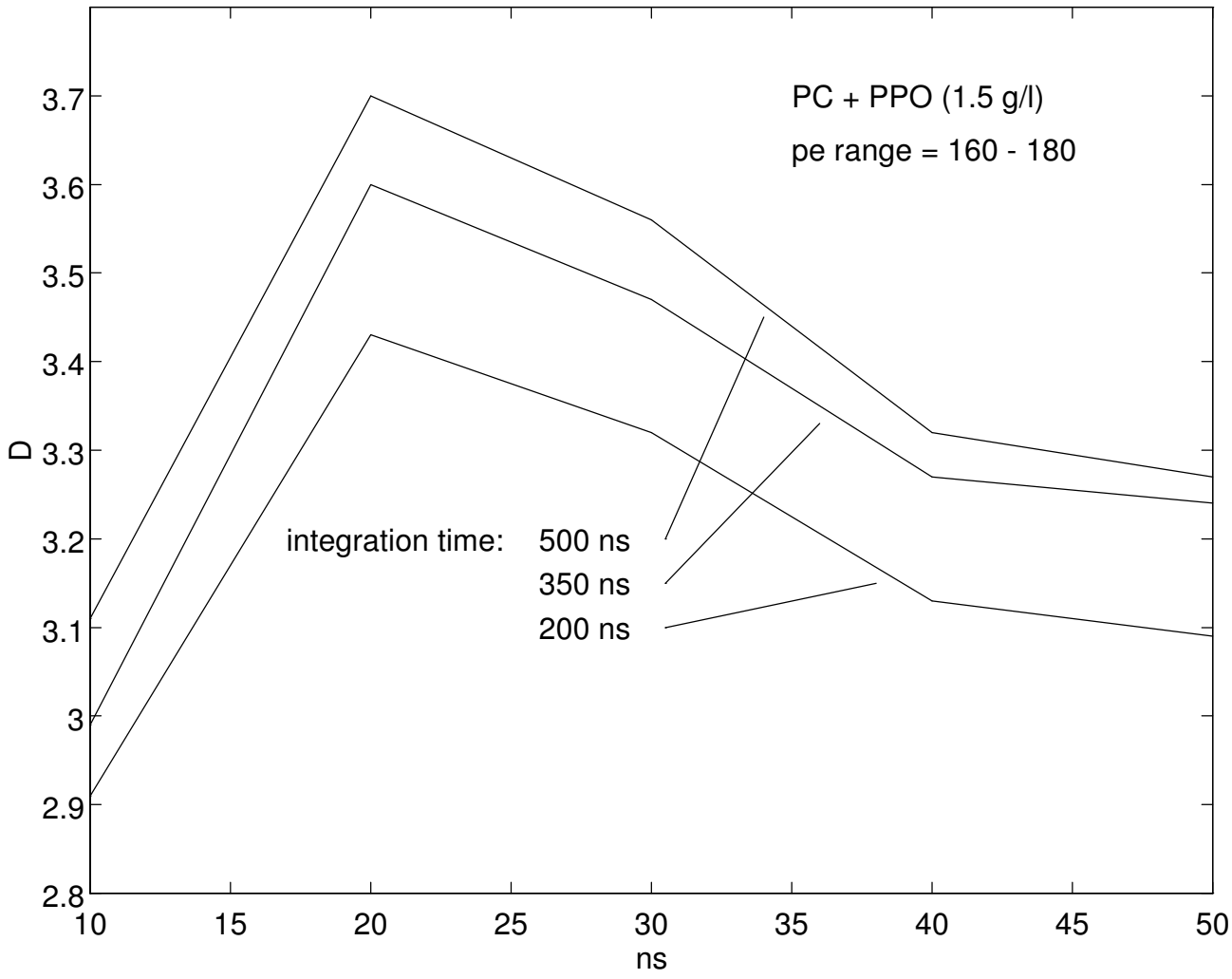
PC + PPO (1.5 g/l)
pe range = 160 - 180
integration time:
500 ns
350 ns
200 ns
D
ns
3.7
3.6
3.5
3.4
3.3
3.2
3.1
3
2.9
2.8
10
15
20
25
30
35
40
45
50

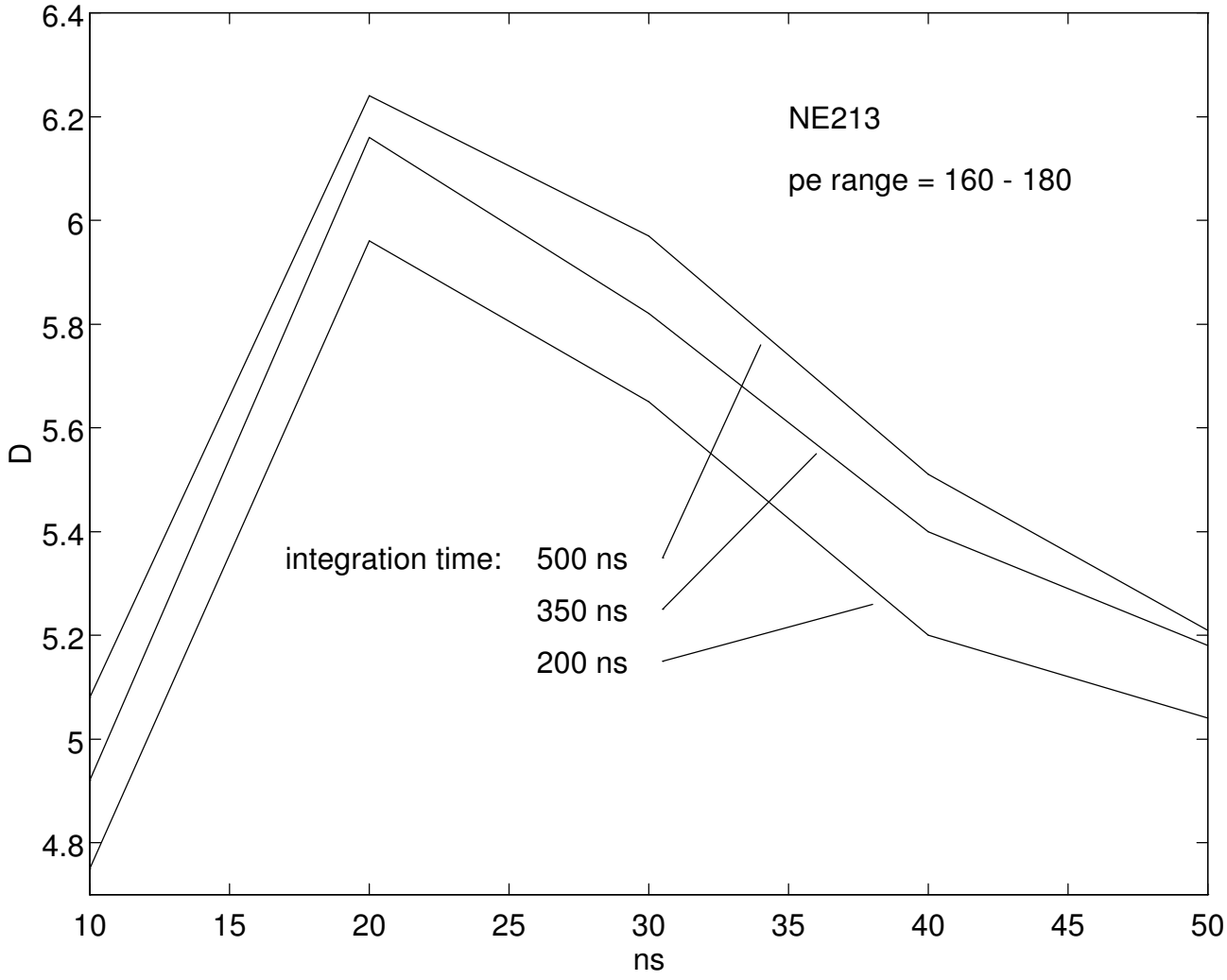
NE213
pe range = 160 - 180
integration time:
500 ns
350 ns
200 ns
D
ns
6.4
6.2
6
5.8
5.6
5.4
5.2
5
4.8
10
15
20
25
30
35
40
45
50

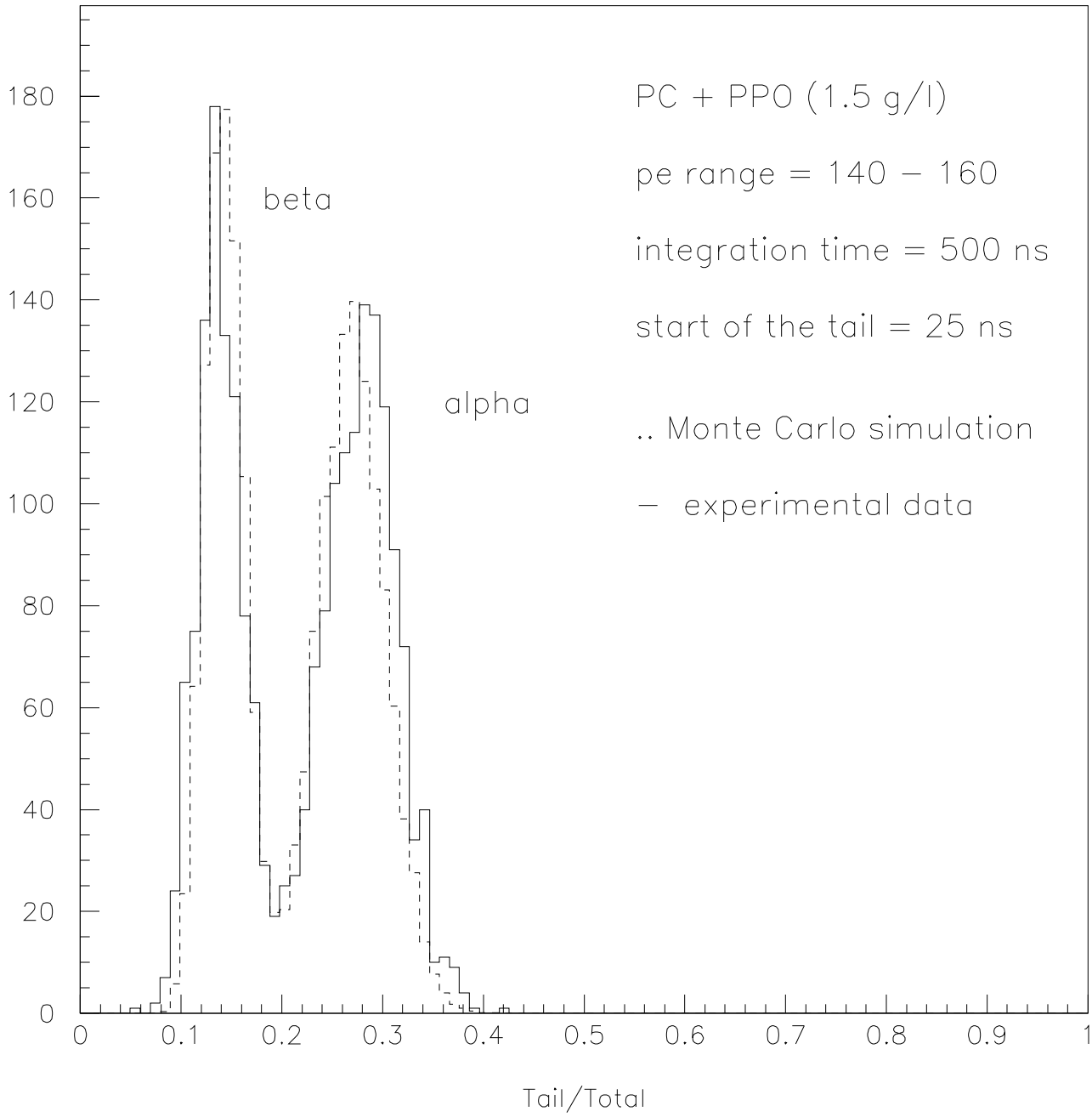
PC + PPO (1.5 g/l)
pe range = 140 – 160
integration time = 500 ns
start of the tail = 25 ns
.. Monte Carlo simulation
– experimental data
beta
alpha
180
160
140
120
100
80
60
40
20
0
0
0.1
0.2
0.3
0.4
0.5
0.6
0.7
0.8
0.9
1
Tail/Total

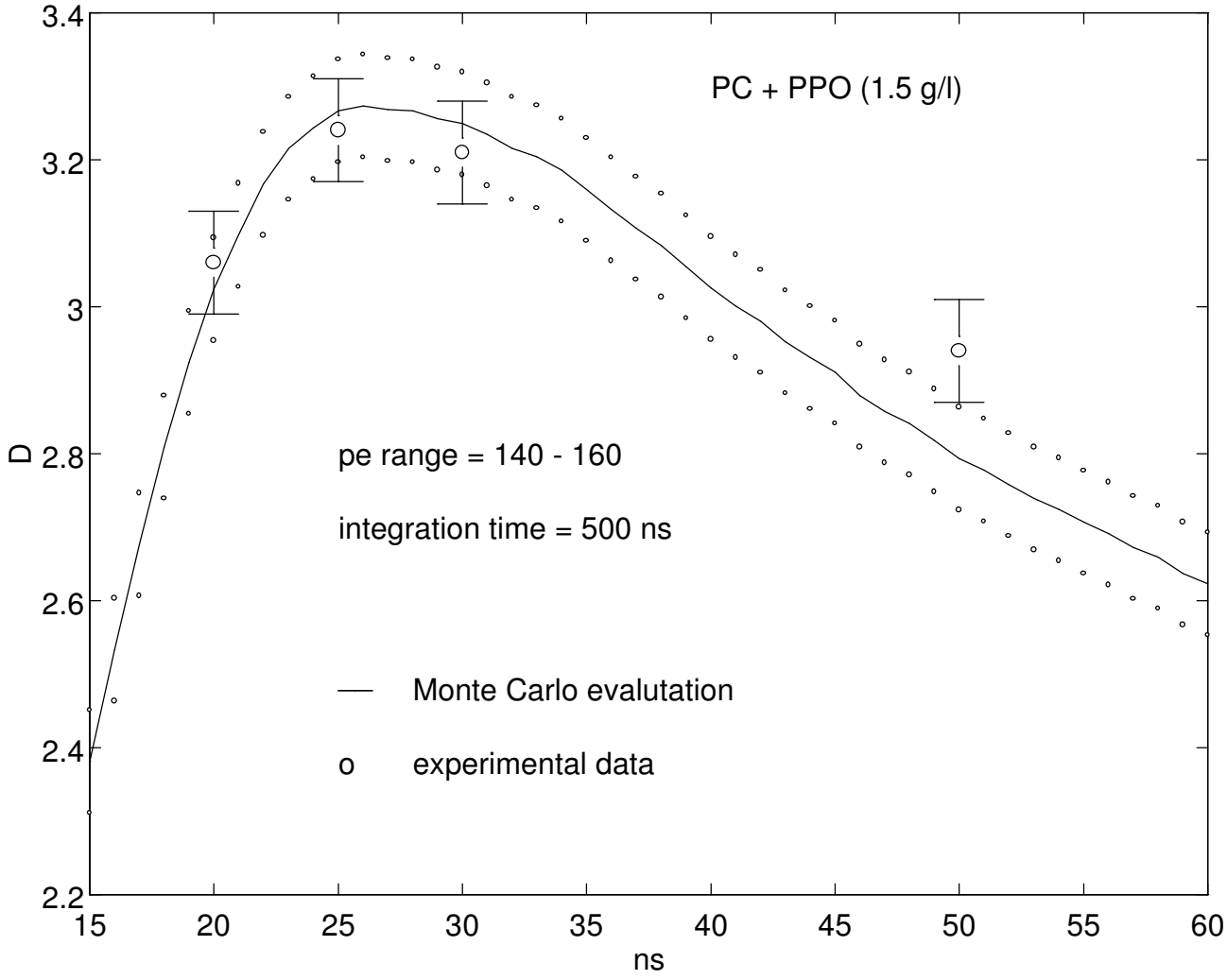
PC + PPO (1.5 g/l)
pe range = 140 - 160
integration time = 500 ns
Monte Carlo evalutation
experimental data
D
ns
3.4
3.2
3
2.8
2.6
2.4
2.2
15
20
25
30
35
40
45
50
55
60